Chapter 3. COUPLING SMALL-SCALE PHYSICAL PROCESSES WITH BIOLOGY

HIDEKATSU YAMAZAKI

Tokyo University of Fisheries

DAVID L. MACKAS

Institute of Ocean Sciences

KENNETH L. DENMAN

University of Victoria

Contents

1. Introduction

Living marine organisms have spent most of their evolutionary time history as single cells, at scales dominated by viscous force. As life evolved toward a larger and more mobile multicelled organism, inertial forces also became important. Hence, microscale organisms in the ocean have experienced small-scale fluid motions throughout their entire existence on Earth. In this chapter we consider how microscale organisms interact with small-scale physics in the ocean, based on current knowledge. We focus our attention on how the behavior of planktonic organisms might be affected by the immediate flow field; hence, we target the behavior of individual motile plankton.

The dynamics of the upper ocean are complex, not the least because of air–sea interaction processes. Winds cause various physical processes, which are not mutually independent: waves, currents, turbulence, and coherent flow structures such as

The Sea, Volume 12, edited by Allan R. Robinson, James J. McCarthy, and Brian J. Rothschild
ISBN 0-471-18901-4

Langmuir circulation. Convection further complicates the dynamics. Thus, the study of trophodynamic interactions among organisms in the upper ocean is a difficult but challenging subject. Clearly, the initial step toward understanding the role of our target organisms, motile plankton, is to establish on matching scales of the distribution of these organisms with simultaneous measurements of the physical environment, including turbulence intensity. The effects of physical processes on phytoplankton, which are for the most part passive, is treated in more detail in Chapter 2.

The distribution of plankton populations has always been an important subject in biological oceanography. At scales of meters to tens of kilometers, spatial heterogeneity (patchiness) and its physical and biological causes and consequences have been extensively discussed and reviewed (see, e.g., Cassie, 1963; Denman and Powell, 1984; Mackas et al., 1985; see also Chapters 4 and 5). However, at the smaller spatial scales that are the subject of this review, plankton patchiness and its interaction with physical processes have been much less studied. This gap is due primarily to technical difficulties of observing meter- and smaller-scale biological spatial structure, although new sampling technologies [such as those described in the Cowles and Donaghay (1998) "Thin Layers" issue of *Oceanography*] are beginning to change this situation. We know that the persistence time scale of microscale patchiness is substantially shorter than for large-scale distributions, that effects of microscale patchiness are likely to influence the mortality and growth of larval fish (Owen, 1989), and that small and microscale patch formation is likely to involve an important behavioral component (Mackas et al., 1985; Folt and Burns, 1999). Unfortunately, only limited information on how individual plankters behave in response to their environment is available from field observations. On the other hand, laboratory observations have enabled a detailed description of zooplankton behavior (Yen and Strickler, 1996; Strickler, 1998; Yen et al., 1998). How much we can extrapolate laboratory observations to actual oceanic conditions is unclear. To bridge the gap between laboratory and field observations, we need to compare and contrast observations from both environments. Because of the scarcity of observations, this comparison is not an easy task for observations of biological behavior but can be done more readily for observations of small-scale physics.

To incorporate the effects of microscale patchiness into ocean ecosystem dynamics, we must be concerned with physical processes at scales comparable with patch sizes, as well as the ambient physical environment of an individual organism. In this chapter we focus our attention on small-scale physics in the upper 100 m of the ocean, where a large fraction of oceanic production and important biophysical coupling among various planktonic organisms occur. Upper ocean processes are forced mainly by winds and solar radiation. In particular, winds induce waves and Langmuir circulations, two processes that are important to mixed layer dynamics. These processes also control turbulence, a ubiquitous phenomenon in the ocean that causes pronounced effects on the environment of planktonic organisms (Yamazaki and Osborn, 1988; Davis et al., 1991). Turbulence has received considerable attention in the biological community since the milestone paper of Rothschild and Osborn (1988). The hypothesis, that "planktonic contact rate increases due to the uncorrelated portion of the turbulent velocity field," is a compelling concept that can bridge the gap between laboratory feeding experiments and field surveys. Although Yamazaki et al. (1991) confirmed the theory of Rothschild and Osborn (1988) through numerical

simulations, they also found that the behavior of organisms could change the contact rates considerably. Yamazaki (1993) considered that a correlated portion of the turbulent velocity field may also be important for the searching and hunting behavior of organisms.

It is useful to distinguish between two rather different ways in which an individual organism can be affected by small-scale physics. The first is one-way influence characterized by a passive "consequence" for the organism. In this category we include instances in which some condition of the local physical environment has an important biological effect but it is known or assumed that the organism does nothing to select the physical conditions and biological consequences it is experiencing. The second, and until recently less studied class of interaction between an organism and its local physical environment is reactive and two-way: The organism experiences a local physical condition and responds in such a way that it alters the probability of encountering this condition (or its biological consequences) in the future. An example is that of migratory selection of a depth stratum with a "preferred" level of turbulence (Mackas et al., 1993). In this class of interaction, the range of spatial and temporal scales for individual response and consequence can be broader than the scale of the physical process that stimulates the response. Relevant biological scales range from body size and immediate sensory sphere, up through longer-term individual ambit and activity scales, to the aggregation of individuals into patches. Although all of these remain much smaller than the spatial and temporal scales of population changes, population dynamics must ultimately depend on events at these smaller individual scales. For both classes of interaction, passive and reactive, we will consider the role of small-scale physical processes in the sensory ecology of zooplankton and their predators (e.g., Dusenbery, 1992), through both modification of sensory cues generated by other biota and physical generation of masking or interfering cues.

In the next section we review small-scale physical processes in the upper ocean. In the subsequent section, the sensory aspects of planktonic organisms are presented. These two sections are required in the coupling between physics and biology. In the final section we examine numerical modeling of planktonic ecosystems, starting from the conventional continuum models and moving toward individual-based models (IBMs).

2. Physical Processes

2.1. Upper Ocean Processes

Mixed Layer Dynamics

The surface layer of the ocean is forced by the atmosphere, land and rivers, and the ocean interior—hence it is the site of a myriad of interacting dynamic physical processes. In the context of coupling small-scale physical processes to biological systems, many physical processes operating in the upper ocean influence the functioning of organisms in the following manner:

1. Stratification and differential turbulent transport maintain phytoplankton cells in sufficient light for photosynthesis.
2. Vertical circulation and the annual cycle of the seasonal thermocline transport nutrients and CO_2 from various depths to the sunlit upper ocean layer.

3. Exchanges with boundaries in the ocean bottom and the coastal regions provide sinks and sources for nutrients, CO_2, O_2, particles, dissolved organic matter, and so on.
4. Currents advect and disperse nutrients, organisms, and organic matter horizontally and vertically.
5. Convergent horizontal currents can concentrate particulates or surface material with densities different from the ambient fluid; that is, positively buoyant particles and surface slicks can be concentrated by surface convergences such as those associated with Langmuir circulation patterns, and negatively buoyant material can be concentrated at depth in convergent upwelling circulation.
6. Small-scale motions affect diffusive exchanges, predator–prey interactions, daily migrations, and so on.

In this chapter we focus on the latter three types of processes, especially the last one, but it is important to remember that other physical processes also contribute to the behavior and dynamics of the planktonic ecosystem.

The mixed layer of the ocean in many ways functions as the boundary layer between the atmosphere and the ocean. There is a strong daily cycle in the mixed layer in most regions of the ocean, as there is in the atmosphere, but there is little sign of daily cycles in the physics of the ocean interior except in the modulation of already exceedingly low light levels. Accepting this premise—that the ocean surface layer (about 100 m thick) is the functioning boundary layer between the atmosphere and the ocean—revised our thinking in a fundamental way. Now, the lower (not readily observable) boundary of the surface ocean layer assumes an importance for vertical exchanges that is comparable with that of the air–sea boundary. For marine organisms, for heat, and for biogeochemical materials such as CO_2 and plant nutrients, exchanges between the surface ocean and the ocean interior are at least as important as the transfer of materials across the air–sea boundary.

Most of the major dynamical processes in the surface oceanic layer that affect marine organisms are depicted in Fig. 3.1. More accurately, these larger-scale driving forces not only transport organisms and materials within the oceanic surface layer but also drive the smaller-scale turbulent motions that cause mixing and that interact with individual phytoplankton, zooplankton, and smaller fish with limited swimming capability. In Tables I and II, we have attempted to show schematically the causal relationships from these larger-scale motions down to the physical processes acting at scales that match the size and activity scales of individual or groups of organisms. Almost all these processes originate from the wind and heat/water/radiation exchanges at the air–sea boundary.

In addition, we now know that the diurnal cycle in solar irradiance strongly modulates both the depth of the active mixing layer and the intensity of turbulent activity within the layer (e.g., Peters et al., 1988; Moum et al., 1989; D'Asaro et al., 1996). It is important to recognize that mixing events lead to a mixed water column. Thus, a mixed layer represents an integrated time history of series of mixing events (Dewey and Moum, 1990). When a water column is completely mixed, a mixed layer can no longer be altered. But mixing within the mixed layer may persist after the water column has homogenized. A mixing layer contains turbulent events, so we call this layer the turbulent mixing layer (TML). This layer should not be treated as a mixed layer (ML). Usually the TML precedes the ML. Figure 3.2 shows a pronounced reduction

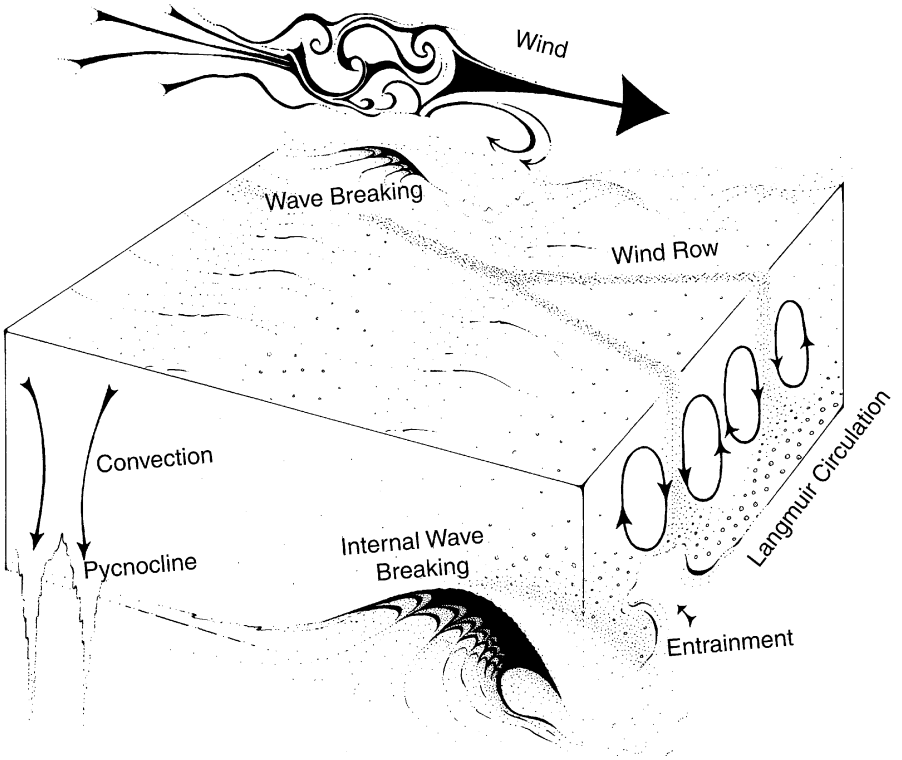

Fig. 3.1. Schematic of the dominant forcing functions and energy-containing motions in the surface ocean mixing layer. (Reprinted with permission from Thorpe, 1985, *Nature*, **318**, 519–522, www.nature.com, copyright 1985, Macmillan Magazines Ltd.)

in the maximum depth reached during daytime heating by a neutrally buoyant float developed by D'Asaro et al. (1996). This diurnal cycle in the depth of the TML and in the energy of the motions within the TML causes important effects on planktonic organisms, on the entrainment and detrainment of passive properties, and as discussed

TABLE I
Linked Physical Processes in the Surface Oceanic Mixing Layer Associated with the Wind, Progressing from the Largest Scale Processes down to Processes That Occur on the Same Scales as the Organisms

Surface waves	→ Breaking	→ Bubbles + turbulence
Surface waves, Current	→ Langmuir cells	→ Vertical mixing/transport
Surface waves, Winds	→ Surface currents	→ Ekman spiral in horizontal currents
Surface currents	→ Vertical shear in ML	→ Shear-induced turbulence
Surface currents	→ Vertical shear at base of ML	→ Breaking internal waves
Surface currents	→ Entrainment	→ Deeping of ML

TABLE II
Linked Physical Processes in the Surface Oceanic Mixing Layer Associated with Heat, Radiation and Moisture (i.e. Buoyancy) Fluxes, Progressing from the Largest Scale Processes down to Processes That Occur on the Same Scales as the Organisms

Buoyancy input	→ Increased stratification	→ Shoaling of ML → Reduced vertical mixing/transport
Buoyancy loss	→ Decreased stratification	→ More efficient wind mixing
	→ Convective overturning	→ Vertical transport and mixing
	→ Penetrative convection	→ Deepening of ML and entrainment of organisms and material from below

later, on the annual cycle of sea surface temperature and the distribution of heat in the upper ocean. Also, and perhaps more important when we discuss motions at the scale of individual plankton, the tracks of the floats illustrate graphically the existence of vertical motions ranging right up to, and probably beyond, the depth of the mixed layer. Thus, planktonic organisms not only experience small vertical displacements associated with diffusive motions within the mixed layer, but must also with some regularity experience displacements over many tens of meters vertically over time scales on the order of an hour.

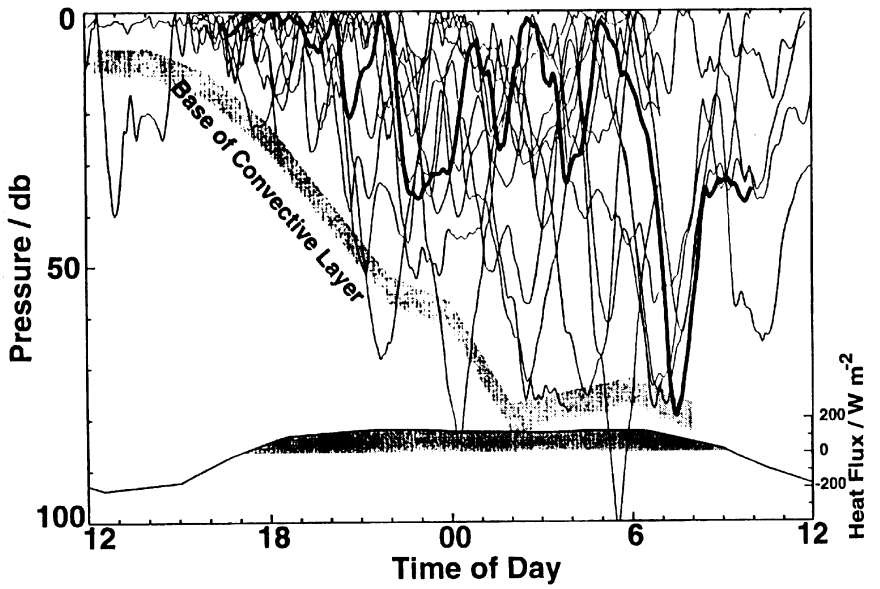

Fig. 3.2. Depth of Lagrangian floats deployed in a diurnally varying convective mixed layer. The average surface heat flux estimated from standard meteorological instruments is plotted at the bottom. The average depth of the convective layer, estimated from the depth of a very weak maximum in stratification from conductivity-temperature-depth (CTD) data, is shown by the shaded region. (From D'Asaro et al., 1996.)

Coherent Flow Structures at the Scale of the Mixed Layer

There is increasing observational evidence that three-dimensional coherent flow structures, with cross-sectional and vertical dimensions comparable with the thickness of the mixed layer, influence both the vertical transport of planktonic organisms and the vertical mixing within the upper ocean (Farmer and Li, 1995; D'Asaro et al., 1996). In the atmospheric boundary layer, these structures are usually referred to as large eddies. In the ocean the most studied of these motions are Langmuir circulation patterns, horizontally aligned vortices in the surface layer roughly parallel to the wind direction, first observed in lakes by Langmuir (1938). Because of the confounding effects of surface waves in the ocean, awareness of Langmuir circulation patterns, and observations of their magnitudes, spatial and temporal structures had to await the development of appropriate sensors and sensor platforms that minimized contamination from surface waves and associated orbital circulations.

Pollard (1977) reviewed the observations, mostly qualitative, and theories of Langmuir circulations up to that time. Subsequently, the development of propeller-based vector-measuring current meters and their deployment from stable platforms (Weller et al., 1985; Weller and Price, 1988), and the development of narrow-beam high-frequency acoustics using bubbles as reflectors, deployed vertically and sideward (e.g., Thorpe, 1984; Pinkel and Smith, 1987; Zedel and Farmer, 1991; Smith, 1992; Farmer and Li, 1995), have rapidly provided both a graphic description of the structure of Langmuir circulations and quantitative estimates of spatial extent, downward speeds, and their evolution in time. Generally, Langmuir circulations may exist in the ocean when wind speeds exceed 3 m s^{-1}. They can drive smaller-scale turbulence in the upper ocean and may be the main transport mechanism moving passive organisms over the entire thickness of the ML during the daytime (in the absence of convective mixing). Langmuir circulations are highly dynamic—constantly bifurcating and coalescing and spanning a range of sizes. They can cause initial rapid deepening of the mixing layer under conditions of weak stability and shear at the base of the mixing layer (Li et al., 1995; Li and Garrett, 1997).

The prevailing theory explaining the generation of Langmuir circulation is based on Craik and Leibovich (1976), who formulated an instability based on the nonlinear interaction between the surface wave–forced Stokes drift and the frictional wind drift current. Recent refinements to this theory have taken into account the expanding body of high-quality observations (e.g., Li and Garrett, 1993, 1995; Leibovich and Tandon, 1993; Tandon and Leibovich, 1995). Finally, Skyllingstad and Denbo (1995) and McWilliams et al. (1997) have put three-dimensional simulations of Langmuir circulations into the context of large eddy simulation (LES) theory, thereby identifying Langmuir circulations as existing within a more general class of coherent flow structures.

Entrainment and Detrainment

During periods when the active mixing layer is deepening, fluid from below the ML is being entrained into the ML as the base of the ML deepens. During periods when the buoyancy input overrides the mixing from wind and surface heat loss, the deeper ML is no longer driven from the surface, and a newer lighter (warmer and/or fresher) ML forms at a shallower depth. We call this situation detrainment, when waters that were part of the surface mixed layer become isolated from surface effects by formation of a lighter layer near the surface with a density gradient between the two layers greater than the density gradient within either of the layers.

Entrainment is caused by processes associated with wind mixing reaching the base of the active ML, by shear instabilities at the base of the ML, or by water cooled at the surface (or brine rejection on the underside of sea ice) sinking (convection) and accelerating such that it causes further mixing at the base of the ML and exchange of water from below with water from above the deepening ML. Convective entrainment may also include drawing surrounding ML fluid into the sinking water parcel and the sinking of that parcel (due to its momentum) to depths below its own density. Thus, penetrative convection often occurs on larger vertical scales than those usually associated with turbulent mixing. In addition, convection may be associated with a finite number of vertically oriented cells, each of which may penetrate far into the denser fluid below, and hence has been difficult to parameterize as a subgridscale process in numerical models.

The two dominant timescales for modulation of entrainment are the annual and daily cycles. On the annual scale, during the autumn and winter the mixed layer deepens due to increased winds and net surface cooling, entraining water from below that had been isolated from surface effects during the summer season. This deepening and entrainment usually reaches its maximum depth several months after the winter solstice. At that time all waters above that depth are being mixed on time scales on the order of days or less. For the North Atlantic, the maximum depth of entrainment is about 500 m, but for the northeastern Pacific it is only about 150 m or less. Hence, remineralized nutrients dissolved organic matter (DOM), phytoplankton spores, and so on, that may have reached a level below the summer seasonal thermocline in the northeastern Pacific are much more likely to escape reentrainment into the surface layer than in the North Atlantic, where surface-driven winter mixing can reentrain material back into contact with the ocean surface from much greater depths. In the springtime, when the daily averaged buoyancy input overrides the turbulent mixing generated from winds and surface cooling, a new shallow mixed layer is formed and strengthens, usually in an episodic manner, as the fluid below the new mixed layer is detrained. So passive organisms, nutrients, DOM, and so on, that were cycling over the entire water column from the surface to winter ML depth, are partitioned into those captured in the new mixed layer, and hence in contact with the surface and those stranded in the detrained water below the new shallow ML.

During the spring and summer, when the input of buoyancy during the daytime solar heating overrides the turbulent mixing tendencies from the wind and surface cooling, a daily cycle occurs in the entrainment–detrainment process: A daily weak shallow mixed layer is formed which is destroyed each evening by convective mixing. Especially in the spring, this ephemeral layer has both physical and biological consequences. Physically, the seasonal mixed layer develops earlier (Woods and Barkmann, 1986; Zahariev, 1998), and the summer sea surface maximum temperature is greater than if there were no diurnal cycle in the heat input to the surface ocean (Zahariev, 1998). Biologically, the spring bloom in phytoplankton develops earlier because the organisms caught in the daytime shallow mixed layer are subjected to a higher average light intensity and develop higher concentrations of biomass/chlorophyll earlier, a positive biological feedback loop leading to earlier primary production. The increased biomass in shallow layers also leads to shallower absorption of shortwave radiation and hence warming of a shallower, more stable layer, a positive biophysical feedback.

Punctuating these regular cycles modulating entrainment into the ML (and detrainment from the ML) are episodic events, usually on time scales of hours to days,

closely matched to dominant scales of growth and behavior of phytoplankton and zooplankton. The formation of the seasonal thermocline in the springtime is not a gradual monotonic process but rather, a series of low wind heating periods (detrainment) alternating with mixing events (entrainment) caused by higher winds events associated with the passage of storms. Similarly, erosion of the seasonal thermocline in autumn is episodic or discontinuous with sharp deepening events (entrainment) often caused by simultaneous high winds and convective heat loss at the sea surface. In the subtropical gyres especially, episodic entrainment of nutrients into the ML associated with evolving mesoscale eddies can stimulate phytoplankton blooms and subsequent grazing and growth events within the zooplankton (see McGillicuddy et al., 1995a; see also Chapter 4). The average seasonal cycle in ML evolution may be viewed then as an integration over these individual episodic events and the diurnal cycle; and in the planktonic ecosystem, as an integration over the short-term responses to these short-term entrainment–detrainment occurrences within the ML.

Numerical Models of the Mixed Layer

The marine planktonic ecosystem is energized by photosynthetic primary production carried out by phytoplankton, whereby solar energy combines with CO_2 and other essential nutrients to produce organic molecules. Phytoplankton can survive only if two strong vertical gradients overlap sufficiently—they need light from above for photosynthesis and they fulfill their requirements for nutrients primarily through nutrients advected and diffused upward from below the sunlit surface layer. So it should not be surprising that physical processes controlling the dynamics of the mixed layer also influence and control the time-dependent primary production within the upper ocean. Hence, robust behavior of planktonic ecosystem models will depend on coupling to robust mixed layer modules, either alone or within a multidimensional circulation model. There are generally three classes of mixed layer models, and they have been developed more or less in chronological sequence.

Bulk Models

Bulk models assume the existence of a completely well-mixed surface layer with negligible vertical gradients (e.g., Kraus and Turner, 1967; Denman and Miyake, 1973; Price et al., 1986). The thickness of the mixed layer is calculated each time step after buoyancy inputs (heat and fresh water) by determining the depth at which a bulk Richardson number reaches a critical value below which the density structure is stable. Physical (and biological) properties are usually discontinuous across the base of the mixed layer and a subsequent algorithm may be used to smooth the gradients, employing either a gradient Richardson number or a vertical diffusion coefficient based on the property gradients. Price et al. (1986) and Gaspar (1988) developed bulk models that have performed well when compared against observations.

Turbulent Closure or K-Theory Models

Turbulent closure or K-theory models estimate at each time step and at each vertical grid point a vertical turbulent diffusion coefficient $K(z, t)$ from an analysis of Reynolds stresses, buoyancy fluxes, turbulent kinetic energy (TKE), stability expressions, and mixing lengths. The TKE equation is determined prognostically, but other gradients are determined diagnostically. The level of closure is determined by the highest-order moment that is calculated, not parameterized. The parameterizations result in downgradient diffusive transport, and only local (small-scale) gradients con-

trol the strength of the diffusive transports. The estimated $K(z,t)$ is used to mix scalars—temperature and salinity—and can then be used to mix biological variables. Most models of this type originate from the set of formulations of Mellor and Yamada (1974, 1982). The development of these models applied to the surface ocean mixing layer can be traced through the widely used models of Mellor and Durbin (1975), Gaspar et al. (1990), and Kantha and Clayson (1994).

Hybrid Models

For the most part, TKE models do not parameterize the large vertical motions within the surface mixing layer, especially those associated with penetrative convection. However, hybrid models employ some nonlocal representations developed from large eddy simulation (LES) modeling, whereby diffusive mixing within the mixing layer scales according to an initial estimate of the thickness of the mixing layer. In addition, hybrid models represent some triple products with parameterizations that result in countergradient fluxes, especially during convective conditions caused by surface buoyancy losses. They may also include parameterization of increased entrainment due to Langmuir circulations, resulting in more rapid or greater deepening of the mixing layer, especially when the layer is already deep and there is otherwise a small wind-driven shear at its base. Two models that exemplify these modifications are Large et al. (1994) and D'Alessio et al. (1998).

Performance of ML models, as compared with observations, has been the topic of numerous papers. The most widely used models are Mellor–Yamada levels 2 and 2.5, the bulk model of Price et al. (1986), and the hybrid model of Gaspar et al. (1990). The most thorough comparison between models has been carried out by Large et al. (1994). Generally, modifications to MY models try to increase the deepening through enhancement of turbulence generated by internal waves in the density gradient below the base of the mixed layer. The hybrid models achieve this through enhanced background diffusion, nonlocal mixing parameterizations, and effects of Langmuir circulations. Zahariev (1998) has shown that simulated heaving by internal waves characteristic of the thermocline modifies mixed layer behavior in a manner analogous to the commonly used value for background diffusion (1 to 2×10^{-5} m^2 s^{-1}), and that models not including daily heating and cooling do not agree with the observed annual cycle in plots of heat content versus sea surface temperature (SST) from ocean weather station (OWS) observations.

2.2. *Turbulence*

Although we experience turbulence often in our daily life, turbulence has evaded any simple mathematical formulation. It is more practical to identify the characteristics of turbulent flows (Tennekes and Lumley, 1990). First, turbulence is disorderly; there exist no identifiable features. It is unpredictable, making it difficult to apply a deterministic approach to describe the flow. Rather, one must apply statistical methods. Second, turbulent mixing processes are efficient compared with molecular mixing processes. The efficiency results from both increased shear and the local gradients of scalar properties. Third, vorticity fluctuations are inherently three-dimensional, and vorticity dynamics play a major role in the description of turbulence. Stewart (1969) identified these three characteristics in his historical film lecture.

In addition to these characteristics, Tennekes and Lumley (1990) emphasize that

turbulent flows are flows. Namely, turbulence is not a descriptive feature of fluids. Rather, it is a fluid flow, and any flow must obey the Navier–Stokes equations. Therefore, no matter how disorderly the flow is, the flow is not free from the governing equations. The dynamical condition is expressed as follows:

$$\frac{\partial u_i}{\partial t} + u_j \frac{\partial u_i}{\partial x_j} = -\rho^{-1} \frac{\partial p}{\partial x_i} + \nu \frac{\partial^2 u_i}{\partial x_j \partial x_j} \tag{1}$$

and the kinetic condition is the continuity equation for an incompressible fluid,

$$\frac{\partial u_i}{\partial x_i} = 0 \tag{2}$$

where u_i is the turbulent velocity component for $i = 1$, 2, and 3, ρ the density fluid, ν the kinematic viscosity, and p the pressure. The coordinate system follows a conventional vector notation for x_i (Kundu, 1990). Thus, a rather simple set of equations produces a complicated flow state, turbulence. Two terms should be noted: the second term of the Navier–Stokes equations is the nonlinear term, which can generate complicated phenomena; and the last term is the viscous term, which dampens small-scale motions and converts the kinetic energy into heat.

To sustain the intensity of turbulence, one must apply external forcing to overcome the loss of kinetic energy due to viscosity. An energy-cascading process from larger eddy motions supplies the kinetic energy lost to dissipation by viscosity at molecular scales. The inertial force of the flow sustains the flow state, whereas the viscosity of the fluid acts to smooth out the fluid shear of the flow. The Reynolds number Re is a ratio between the inertial force and the viscous force and is defined by the characteristic length scale of the flow L, the velocity scale V, and the kinematic viscosity of fluid ν:

$$\mathrm{Re} = \frac{LV}{\nu} \tag{3}$$

The inertial force is the driving force of turbulence, and the viscous force is a suppressing agent. Vigorous turbulence requires a large Reynolds number, usually of order 1000 or more. Dynamically speaking, a flow with a high Reynolds number exhibits processes that are highly nonlinear, and disorder results from the chaotic nature of the nonlinear processes.

Microscales

Although turbulent flow is complex, there are a few successful theories that generalize the nature of the flow. The most important one, the inertial subrange theory of Kolmogorov (1941a), predicts a universal spectral slope in the wavenumber range $L_0^{-1} \ll k \ll \eta^{-1}$, where L_0 is the spatial scale of external forcing and η is the Kolmogorov microscale. Since the range between these two scales has to be large by the definition of the inertial subrange, the associated Reynolds number also has to be large (Kundu, 1990). There the velocity power spectrum follows a $k^{-5/3}$ universal shape. Within this range of flow scales, the actual size of the flow features is not

important for the cascading process of the turbulent energy. The first evidence for the existence of the inertial subrange came from oceanic turbulence observations (Grant et al., 1962).

The Kolmogorov length scale is defined from a simple dimensional argument: that the smallest eddy should be determined from a combination of the kinetic energy dissipation rate ϵ and the viscosity of the fluid ν:

$$\eta = (\nu^3/\epsilon)^{1/4} \tag{4a}$$

The same two properties can be combined to produce the Kolmogorov velocity scale:

$$\nu_K = (\epsilon\,\nu)^{1/4} \tag{4b}$$

and the Kolmogorov time scale:

$$\tau_K = (\nu/\epsilon)^{1/2} \tag{4c}$$

The rate of the kinetic energy dissipation ϵ is the most important observable parameter describing the dynamics of turbulence. In general, ϵ comprises 12 independent terms:

$$\epsilon = 2^{-1}\nu \left\langle \left(\frac{\partial u_i}{\partial x_j} + \frac{\partial u_j}{\partial x_i} \right)^2 \right\rangle \tag{5}$$

where $\langle\cdot\rangle$ is the ensemble averaging operation (i.e., average over many independent realizations) (Kundu, 1990). Fortunately, due to the law of physics, the flow field approaches an isotropic state as the Reynolds number increases. Then a single-component turbulent shear can represent the sum of all terms if isotropy is assumed. Under isotropy, we can estimate ϵ from a cross-stream shear component such that

$$\epsilon = 7.5 \left\langle \left(\frac{\partial u_1}{\partial x_3} \right) \right\rangle \tag{6}$$

where the index 3 is usually taken in the vertical direction. The Reynolds number Re_0, based on the external forcing scale L_0, is reasonably large for geophysical flows. For example, a 0.1 m s^{-1} friction velocity due to wind stress exerted on a 1-m-thick shear layer gives 10^5 for the corresponding Reynolds number. On the other hand, the Reynolds number based on the Kolmogorov scale is always 1 by definition. Another important scale is the Taylor microscale λ, which is relevant to the local structure of turbulent flows and is defined as (Tennekes and Lumley, 1990)

$$\lambda^2 = 2\langle u_1^2 \rangle \left\langle \left(\frac{\partial u_1}{\partial x_3} \right) \right\rangle^{-1} \tag{7}$$

Since this scale does not explicitly contain the external scale, it is a convenient measure to compare different forcing conditions of turbulent flows. A Reynolds number Re_λ based on λ is usually much smaller than Re_0. Roughly speaking, the two are related as follows (Levich, 1987):

$$\mathrm{Re}_0 \approx \mathrm{Re}_\lambda^2/8 \tag{8}$$

For the example given above, the corresponding Re_λ is about 900.

Thorpe (1977) proposed a length scale l_T, which characterizes the energy-containing eddy size based on a sorted density profile, whereby observed densities are exchanged vertically until a stable density profile is obtained. The Thorpe scale is a good length scale to describe the size of an overturning eddy for a stratified fluid. The intensity of stratification is expressed in terms of a buoyancy frequency,

$$N = \left(-g\rho^{-1} \frac{\partial \rho}{\partial x_3} \right)^{1/2} \tag{9}$$

where g is gravity acceleration, ρ the density of the fluid, and x_3 the vertical coordinate. When an eddy scale exceeds l_T, the eddy is no longer free from the effect of gravity. A combination of ϵ and N provides another length scale characterizing an overturning eddy size, the Ozmidov scale, $l_O = (\epsilon/N^3)^{1/2}$. These two scales correlate closely with each other (Dillon, 1982). The Thorpe scale l_T does not require ϵ but requires a sorting process. On the other hand, l_O requires ϵ and the density profile for N. Since both these scales estimate the overturning scale of individual mixing events, an external length scale L_0 is usually larger than these scales. A reasonable estimate for L_0 is the turbulent patch size L_P. The various length scales used to describe turbulent flow are listed in Table III. Different values for the rate of dissipation of turbulent energy ϵ yield different values for the Kolmogorov scales, as shown in Table IV.

Some microscale velocity variability is biologically driven by swimming and other movements of organisms embedded in the flow field. Examples include the wakes and feeding currents of individual mesozooplankton and nekton, and localized upwelling or downwelling cells (bioconvection) produced by the aligned "prop-

TABLE III
Length Scales[a]

L	Characteristic Length Scale
L_0	External forcing scale
L_p	Turbulence patch size
l_T	Thorpe scale
l_O	Ozmidov scale
λ	Taylor microscale
η	Kolmogorov scale

[a] In general, the following inequality is true: $L_p \approx L_0 \geq l_T \approx l_O \geq \lambda \geq \eta$.

TABLE IV
Kolmogorov Scales for Kinematic Viscosity $\nu = 10^{-6}$ m^2 s^{-1}

ϵ [W kg^{-1} (cm^2 s^{-3})]	η (m)	ν_K (m s^{-1})	τ_K (s)
10^{-4} (1)	3.16×10^{-4}	3.16×10^{-3}	1.0×10^{-1}
10^{-5} (10^{-1})	5.62×10^{-4}	1.78×10^{-3}	3.16×10^{-1}
10^{-6} (10^{-2})	1.0×10^{-3}	1.0×10^{-3}	1.0
10^{-7} (10^{-3})	1.78×10^{-3}	5.62×10^{-4}	3.16
10^{-8} (10^{-4})	3.16×10^{-3}	3.16×10^{-4}	10.0
10^{-9} (10^{-5})	5.62×10^{-3}	1.78×10^{-4}	31.6
10^{-10} (10^{-6})	1.0×10^{-2}	1.0×10^{-4}	100

wash" of highly aggregated microorganisms. Although the kinetic energy associated with these motions is normally extremely small, we note that the resulting flow patterns can provide biologically important sensory information and aggregation cues and mechanisms (see Sections 3 and 4).

Intermittency

The year 1941 stands out in the history of the turbulence study: Kolmogorov (1941b) also proposed another important concept in the theory of turbulence. He applied the lognormal distribution to study the size distribution of crushed rocks, which were broken into several pieces at a time from a single stone. Gurvich and Yaglom (1967) extended the lognormal theory to a turbulent energy process. The theory predicts that a locally averaged ϵ will follow a lognormal distribution. In an effort to make the theory simple, Gurvich and Yaglom (1967) assumed that the averaging scale r satisfies $\eta \ll r \ll L_0$ and that the statistical variability for ϵ within the external length scale domain L_0 is homogeneous. Then, $\log \epsilon_r$, the logarithm of locally averaged dissipation rate over a spatial scale r, follows a normal distribution. The theory is useful for predicting the statistical nature of ϵ_r, since it only requires two parameters, the mean and the variance of $\log \epsilon_r$.

The model is developed by considering a domain Q, with energy-containing eddy size L_0, where Q is proportional to L_0^3. The volume-averaged dissipation rate is denoted $\langle \epsilon \rangle$ and defined as

$$\langle \epsilon \rangle = Q^{-1} \int_Q \epsilon(\mathbf{x})\, d\mathbf{x} \tag{10}$$

The original domain Q is successively divided into subdomains q_i, with length scales l_i. The average dissipation rate in a volume q_i is then

$$\epsilon_i = q_i^{-1} \int_{q_i} \epsilon(\mathbf{x})\, d\mathbf{x} \tag{11}$$

The breakage coefficient α_i is defined as the ratio of two successive ϵ_i:

$$\alpha_i = \frac{\epsilon_i}{\epsilon_{i-1}} \tag{12}$$

for $i = 1, \ldots, N_b$, where N_b is the number of breakage processes. In the breakage model, the ratio of length scales l_{i-1} and l_i for two successive breakages is a constant,

$$\lambda_b = \frac{l_i}{l_{i-1}} \tag{13}$$

Let l_{N_b} be r and ϵ_{N_b} be ϵ_r, respectively. The volume average dissipation rate ϵ_r can be expressed in terms of $\langle\epsilon\rangle$:

$$\log\ \epsilon_r = \log\langle\epsilon\rangle + \sum_{i=1}^{N_b} \log\ \alpha_i \tag{14}$$

By virtue of the third hypothesis of Kolmogorov (1962), the members of the set [log $\alpha_i, \ldots,$ log a_{N_b}] comprise mutually independent, identically distributed random variables. Gurvich and Yaglom (1967) assumed that the random variable log α_i follows a normal distribution; thus α_i is lognormal. Gurvich and Yaglom (1967) then showed that log ϵ_r is also lognormal by applying the central limit theorem to the right-hand side of equation 14. Since α_i is the ratio of two successive volume-average dissipation estimates, this value has a certain upper limit, but the lognormal distribution does not. However, higher-order statistics for turbulent velocities are significantly affected by the upper tail of this probability density function for α_i. To avoid this problem, Yamazaki (1990) instead applied the beta distribution (Mood et al., 1974), whose domain is supported by a finite range for α_i. Although Gurvich and Yaglom's lognormal model does not follow experimental values for higher-order statistics of turbulent velocities (Anselmet et al., 1984), Yamazaki's model shows good agreement up to 18th-order statistics. Higher-order statistics are important in characterizing the dynamics of turbulence, but low-order statistics such as mean and variance of log ϵ_r are indistinguishable between the two models. The mean m_r and the variance σ_r^2 of log ϵ_r are

$$m_r = \log\langle\epsilon\rangle + \xi \log_\lambda(Lr^{-1}) \tag{15}$$

$$\sigma_r^2 = \mu \log_\lambda(Lr^{-1}) \tag{16}$$

where $\log_\lambda$ (Lr^{-1}) is the number of breakage processes N_b, and ξ and μ are the mean and variance of log α. The purpose of this section is not to provide an in-depth discussion of the lognormal theory (see, e.g., Yamazaki, 1990); rather, we intend to introduce a simple tool to predict the mean and variance of the dissipation rate for the subdomain r^3 within the mother domain. Gurvich and Yaglom (1967) provided a simple relationship between ξ and μ as follows:

$$\xi = -\tfrac{1}{2}\mu \tag{17}$$

When the breakage ratio is roughly 3, $\log_\lambda(Lr^{-1}) \approx \log_e(Lr^{-1})$. Numerous experiments show μ to be between 0.2 and 0.3. For the sake of simplicity, we take 0.25 for this value. We then arrive at the following relationship for the local average dissipation rate ϵ_r and the domain average dissipation rate $\langle\epsilon\rangle$:

$$m_r = \log\langle\epsilon\rangle - 0.125\log(Lr^{-1}) \tag{18}$$

$$\sigma_r^2 = 0.25\log(Lr^{-1}) \tag{19}$$

The probability density function of ϵ_r is lognormal with these parameters; thus we can estimate the statistical characteristics of locally averaged dissipation rate.

Oceanic Observations

Turbulence occurs everywhere in the ocean, but the intensity varies in time and space. The past two decades of microstructure observations have yielded a significant body of information on the nature of oceanic turbulence. In general, turbulence exhibits a layered structure and patchiness, just as do plankton. The intensity is normally high near an interface, which can be either external or internal. The sea surface and the ocean floor are external interfaces; a sharp density step in a thermocline is an internal interface.

The turbulent intensity in a mixed layer may exhibit a simple depth-dependent profile due to pure wind forcing (Fig. 3.3). A dissipation rate as high as 10^{-5} W kg^{-1} just below the surface during 12 m s^{-1} winds shows good agreement with the theory. Oakey and Elliott (1982) also demonstrated that a constant stress layer model is applicable to estimate the average dissipation rate in the mixed layer. But in general, the logarithmic law underestimates the dissipation rates near the surface due to additional stirring mechanisms, such as waves and Langmuir circulation (Kitaigorodskii et al., 1983; Gargett, 1989; Agrawal et al., 1992). Winds cause Langmuir circulations, which create spatially coherent structures within the flow field. The nature of turbulent structures within Langmuir circulation is not well known, except for the rate of dissipation of kinetic energy ϵ, which may be high within the convergence zone in Langmuir circulations (Osborn et al., 1992). Surface slicks, an indication of Langmuir circulation, have been widely reported in the literature.

Cooling at the surface also promotes effective vertical mixing and complicates the prediction of turbulence intensity compared with the simple wind forcing case (Gregg, 1987). For convectively dominated mixing conditions, Shay and Gregg (1986) showed that dissipation rates in the mixed layer follow a buoyancy flux scaling law. Nighttime convection and daytime solar heating establish a diurnal cycle in the surface mixed layer (Moum et al., 1989; Anis and Moum, 1992). In some extreme cases, convection creates a significantly deeper mixing layer. For example, during winter in the Gulf of Aqaba, an isopycnal layer has penetrated as deep as 800 m, and phytoplankton cells were physiologically uniform from the surface down to at least 400 m (Genin et al., 1995).

Another important feature of mixing in the upper surface boundary layer is caused by near-inertial waves, which are generated at the base of mixed layer during the passage of a storm. For example, a turbulent layer at the base of a mixed layer shown in Fig. 3.4 is completely separated from a wind-induced turbulent layer near the surface. The layer is slightly below the base of the mixed layer; therefore, it is not

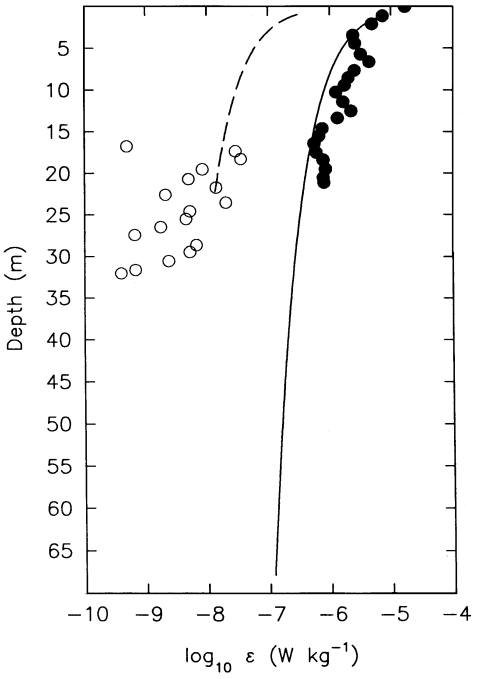

Fig. 3.3. Comparison of observed dissipation rates and the predicted dissipation rates from the Ekman layer model. Turbulence was measured from the submarine USS *Dolphin* in Monterey Bay, California. During the experiment, the *Dolphin* stayed within the mixed layer. The dissipation rates shown in this figure are 1-m-depth averaged values. At the beginning of the experiment, winds were mild (4 m s^{-1}) and the observed dissipation rates (open circle) near the bottom of the Ekman layer (dashed line) are in agreement. Passage of a weather front soon after the dive caused a high wind speed (12 m s^{-1}), and 5 h later the mixed layer would have reached more than 30 m (solid line: the Ekman layer). Although the observed dissipation rates (solid circle), in general, slightly exceed the predicted values, the tendency of dissipation in the mixing layer is obvious. (Reprinted from *Deep-Sea Res.*, Vol. 47, Haury et al., "Effects of Turbulent Shear Flow on Zooplankton Distribution," pp. 447–461, Copyright 1990, with permission from Elsevier Science.)

generated from shear associated with the mixed layer interface. From expendable current profiler (XCP) observations, the surface layer motions correlate with a near-inertial wave. In fact, a large fraction of the shear in the upper ocean is generated by near-inertial waves (D'Asaro, 1989), and Price (1981, 1983) discussed near-inertial wave generation due to storms.

Turbulent layers in a thermocline are usually patchy, with thicknesses of normally a few meters (Fig. 3.5). The layers are often separated by sharp density interfaces. Figure 3.6 clearly shows a density interface (internal interface) separating a region of high turbulence from a quiet region. A turbulent layer in a thermocline is considered to be energetic if the dissipation rate exceeds 10^{-8} kg^{-1}. Even two independent sampling profiles separated horizontally by several kilometers "see" similar patches with thickness of no more than 10 m (Fig. 3.7). Such intermittent distribution of turbulent layers must contribute to the patchy distribution of particles at submeter scale. Results of the recent thin layers study (Cowles and Donaghay, 1998) have provided useful information on this interaction. Osborn (1998) discussed physical mechanisms

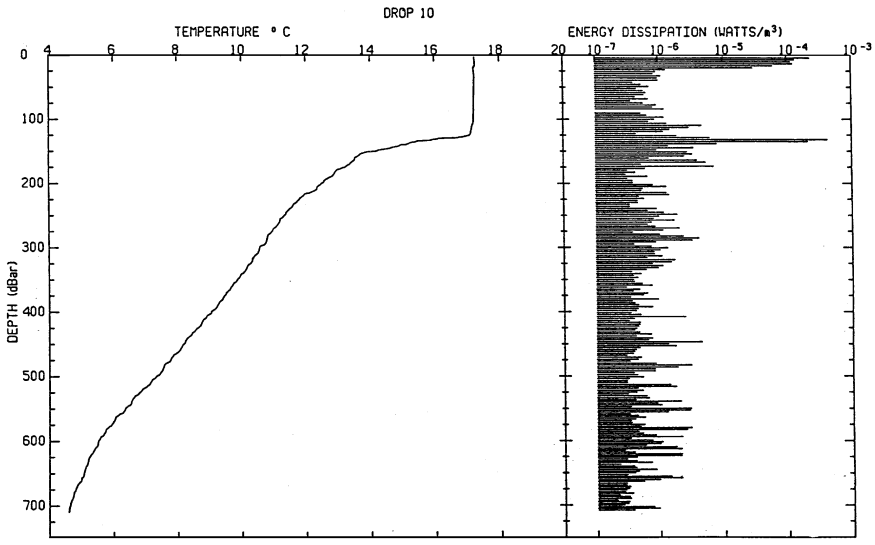

Fig. 3.4. Quasi-isothermal mixed layer that is actively turbulent in only the upper 20 m. The absence of dissipation shows that there is no Reynolds stress between 20 and 130 m depth. The strongest dissipative feature is between 130 and 136 m. This is the depth of a near-inertial wave with a Richardson number of 0.33. (From Lueck, 1988.)

by which thinly layered water column structure can be generated and modified. The vertical extent, horizontal and temporal continuity, and covariance among thinly layered biota and biologically reactive chemicals have been described in 1998 papers by Cowles et al., Hanson and Donaghay, Holliday et al., and Sieracki et al. Direct visual observations of zooplankton distributions (Davis et al., 1992) have shown that actively swimming copepods form colonies of order 10 cm horizonal dimension; the same study showed that the distribution of nonmotile blue green algae exhibits no significant spatial coherence at the same horizontal scale. However, even nonmotile taxa show considerable vertical aggregation at submeter scale. These and similar new observations are exciting and provide a consistent picture that microorganisms, especially zooplankton, are indeed responding to microscale physics.

Haury et al. (1990) showed that the vertical distribution of zooplankton species can be altered selectively depending on their swimming ability. Turbulence intensity may exceed the swimming capability of some species, in which case physics dominates biology. On the other hand, Mackas et al. (1993) reported that some copepods consistently appear in mixing layers, but some other species are observed just below mixing layers. They hypothesize that while some copepods "like" a turbulent regime, others prefer quiet water. In such cases, biology dominates physics.

To gain some idea of how the turbulent velocity field might affect the swimming ability of microorganisms, Yamazaki and Squires (1996) estimated the root-mean-square (rms) turbulent velocity associated with the energy-containing eddy scale by integrating observed turbulent velocity spectra. The integration is done between half the Ozmidov wavenumber and the Kolmogorov wavenumber. Shown in Fig. 3.8 are estimates for the rms velocity and Kolmogorov velocity scale, $v_K = (\epsilon \nu)^{1/4}$. A simple picture is that a turbulent patch comprises many eddies whose velocity scales are in between these two velocity scales. It should be noted that the rms velocity scale is

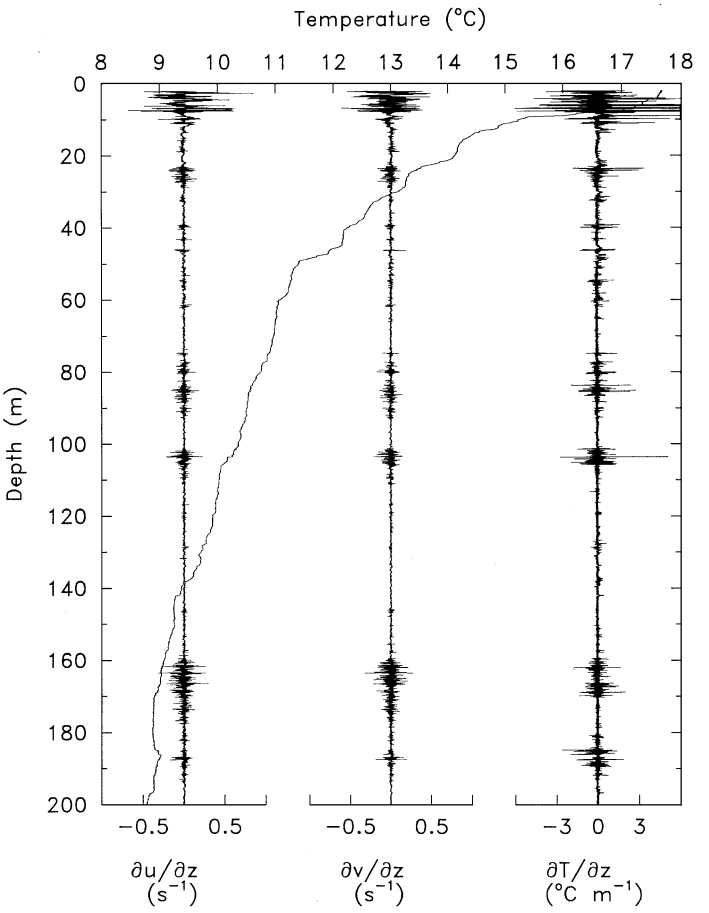

Fig. 3.5. Microstructure profile data obtained from a free-fall instrument *Camel II*. The instrument measures two shears ($\partial u/\partial z$, $\partial v/\partial z$) and vertical temperature gradient ($\partial T/\partial z$) as well as the temperature profile. Although the upper surface layer is still in a stratified condition, turbulence is active in the upper 10 m. A 5-m uniform temperature interface is associated with a turbulent patch at 28 m depth. A strong turbulent patch occurred at 170 m depth, where the California undercurrent is found. The dissipation rate associated with 0.1 s^{-1} rms velocity shear is roughly 7.5×10^{-8} W kg^{-1}; see, for example, 103 m depth. (From Yamazaki and Lueck, 1987.)

not the absolute upper bound of velocity in a given patch. The rms velocity is an average for turbulent velocities; thus occasional bursts in the turbulent velocity field can exceed this value due to intermittency and episodic events much shorter than the data record. However, the rms velocity still gives a good representation of an average velocity scale experienced by microorganisms in the ocean. Another aspect of Fig. 3.8 is that the rms velocity and Kolmogorov velocity scales collapse at a dissipation rate of roughly 10^{-10} W kg^{-1}, which is the noise level of the turbulent shear probe. A turbulence intensity of this level is negligible, and the flow field is almost laminar. A turbulent patch in the seasonal thermocline with a dissipation rate of 10^{-8} W kg^{-1} is 100 times more energetic than the noise level, but the associated velocity scale of 3.16×10^{-4} m s^{-1} (from Table IV) does not exceed the swimming

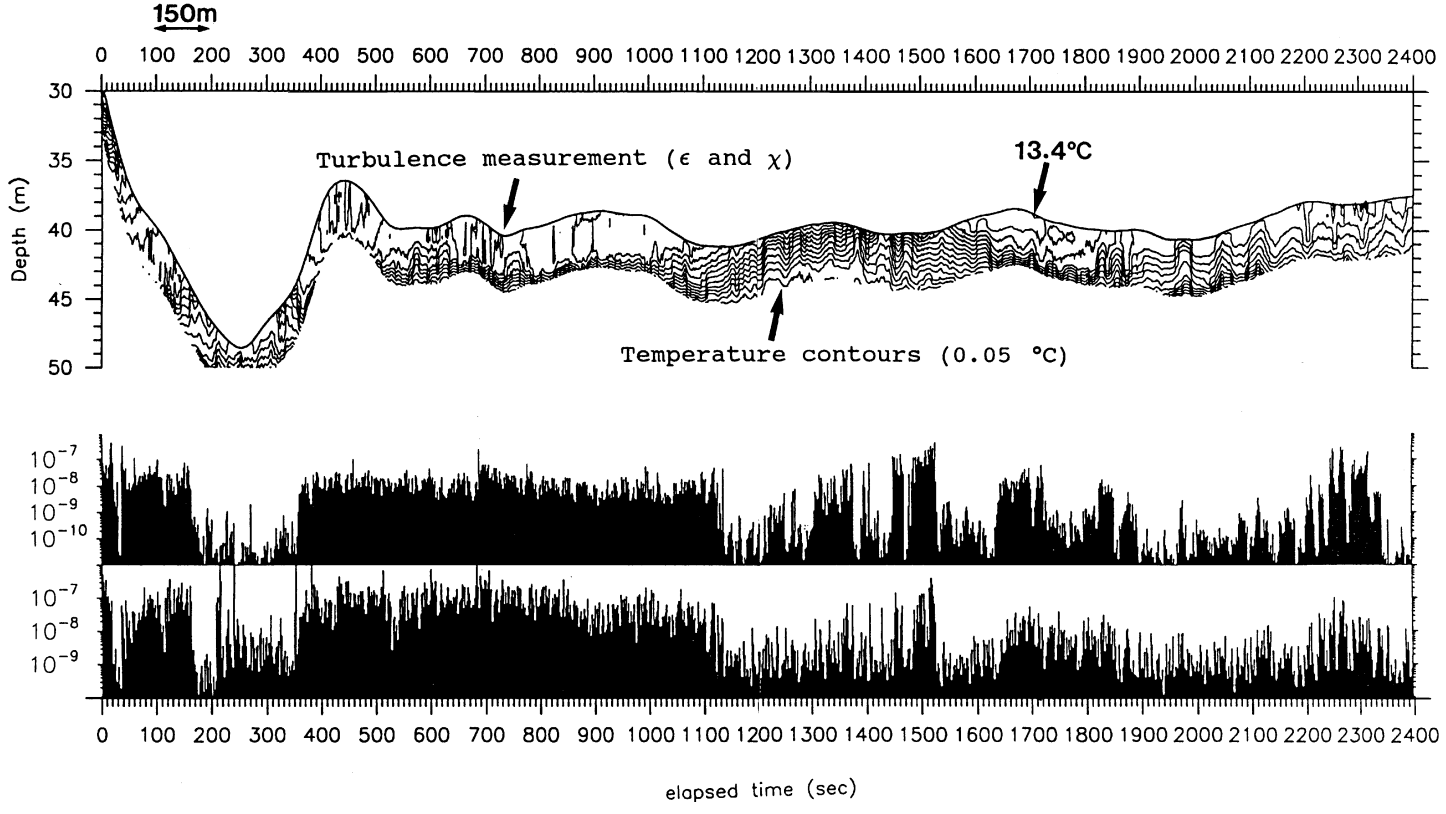

Fig. 3.6 Microstructure data observed from the submarine USS *Dolphin*. A thermister chain mounted on a 5-m tripod at the bow of the submarine provided the thermal structure of the observed area. A thick line at the top of the temperature contour shows the location of microstructure probes. During an elapsed time interval between 0 and 1100 s, a well-mixed layer appeared at 40 m. The turbulent intensity in this layer is high, but as soon as the probes enter a thermally stratified layer, the turbulence level drops to a significantly lower intensity.

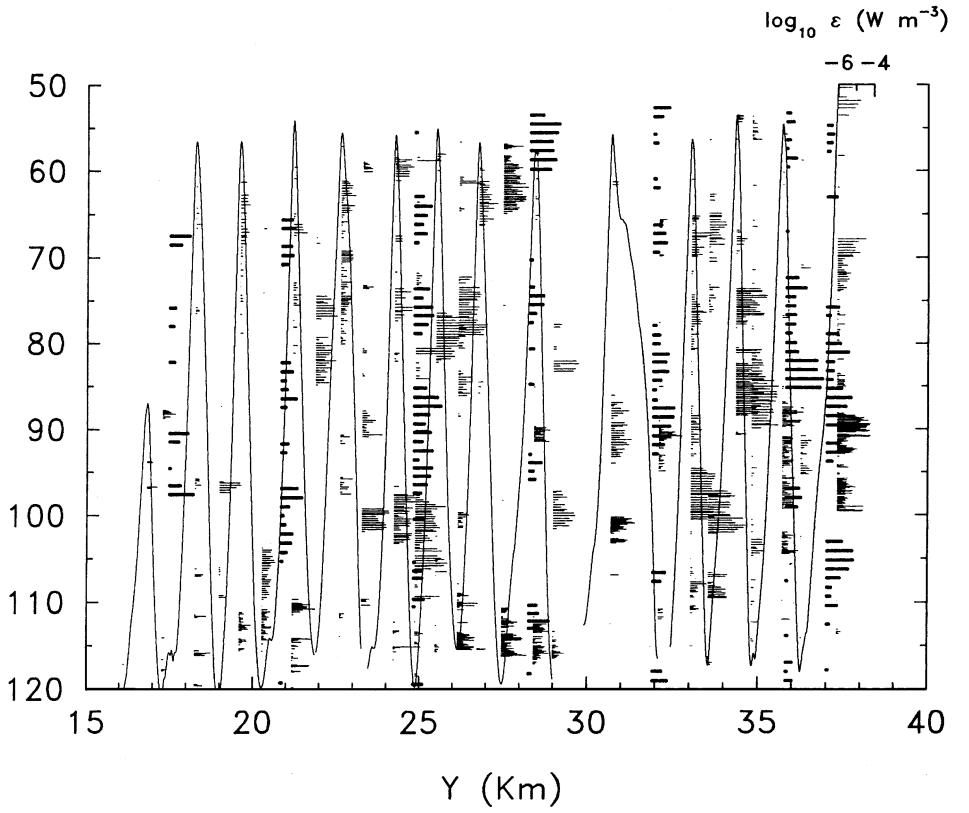

Fig. 3.7. Spatial features of the turbulent field between kilometers 15 and 40 from the USS *Dolphin* (thin bars) and the *Camel* (thick bars). Only values exceeding 10^{-6} W m^{-3} are shown in this figure. The solid line shows the dive track of the *Dolphin*.

abilities of *Euchaeta rimana* and *Metridia pacifica*. Thus, in a turbulent patch in the seasonal thermocline, a large fraction of copepods can probably swim freely without significant influence from turbulent motions.

Physical oceanographers can now measure (with some confidence) the rate of dissipation of turbulent kinetic energy ϵ, although the actual engineering skill is limited to a few groups. While existing data are useful for consideration of the influences of turbulence on trophodynamics, one must realize that a gap exists between the measurement needs of physical oceanographers and the applications of interest to biologists. Normally, what physical oceanographers call an instantaneous dissipation is an average dissipation rate over a certain spatial scale, somewhere around 50 to 100 cm. Physical oceanographers are interested in an extensive average of such "instantaneous" dissipation rates. On the other hand, microorganisms experience a true instantaneous velocity strain field. Figure 3.9 shows the difference between local dissipation rate and 1-m-average dissipation rate. Clearly, local dissipation rates can attain much higher rates than the 1-m average. Yamazaki and Lueck (1990) investigated whether the lognormal distribution theory is applicable to the local dissipation rate. Although the local dissipation rate did not follow the lognormal distribution, an

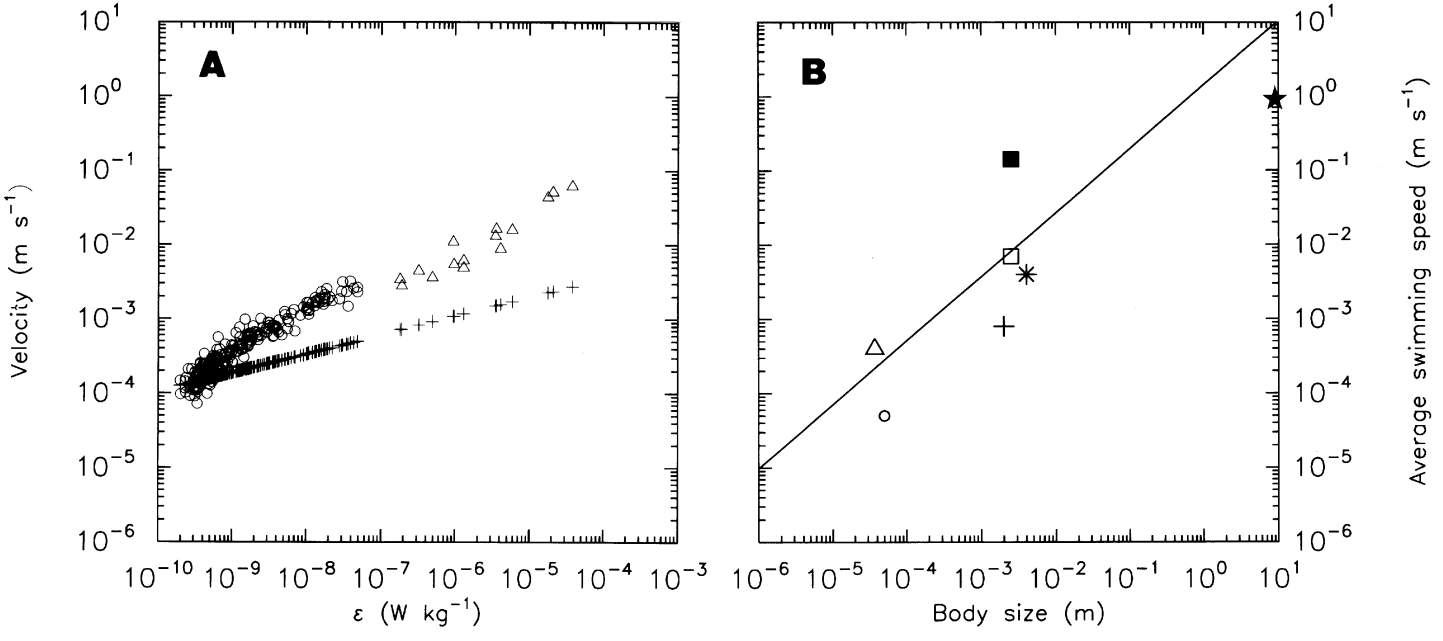

Fig. 3.8 (*A*) Kolmogorov velocity scale (+) and the rms turbulent velocity scale are plotted against observed dissipation rates (ϵ). Open circle samples are from a seasonal thermocline (Yamazaki, 1990), and open triangle samples are observed in a fjord (Gargett et al., 1984). (*B*) Average swimming speeds of various organisms are plotted against body size. Shown are two phytoplankton (open triangle, *Gyrodinium dorsum*; open circle, diatom), three zooplankton (open square, *Euchaeta rimana*; plus sign, *Oithona daisae*; asterisk, *Metridia pacifica*) and a shark (filled star). The filled square denotes escaping swimming speed for *Euchaeta rimana* (Yen, 1988). The empirical relationship between the body size and the nominal swimming speed suggested by Okubo (1987) is shown by solid line.

averaging scale as small as 3η for the dissipation rate reduces to a lognormal distribution (Fig. 3.10). The lognormal distribution predicts a much higher value for the local dissipation rate, but the low values of the observed local dissipation rate appear much smaller than the predicted values from the theory. Since the averaged dissipation rates over 3η distribute lognormally, a velocity shear intensity at this averaging scale can be predicted in a probabilistic sense from theory. The velocity shear field at a smaller length scale does not exceed the predicted value from the lognormal theory. The prediction provides an upper bound for the velocity shear within the minimum averaging volume.

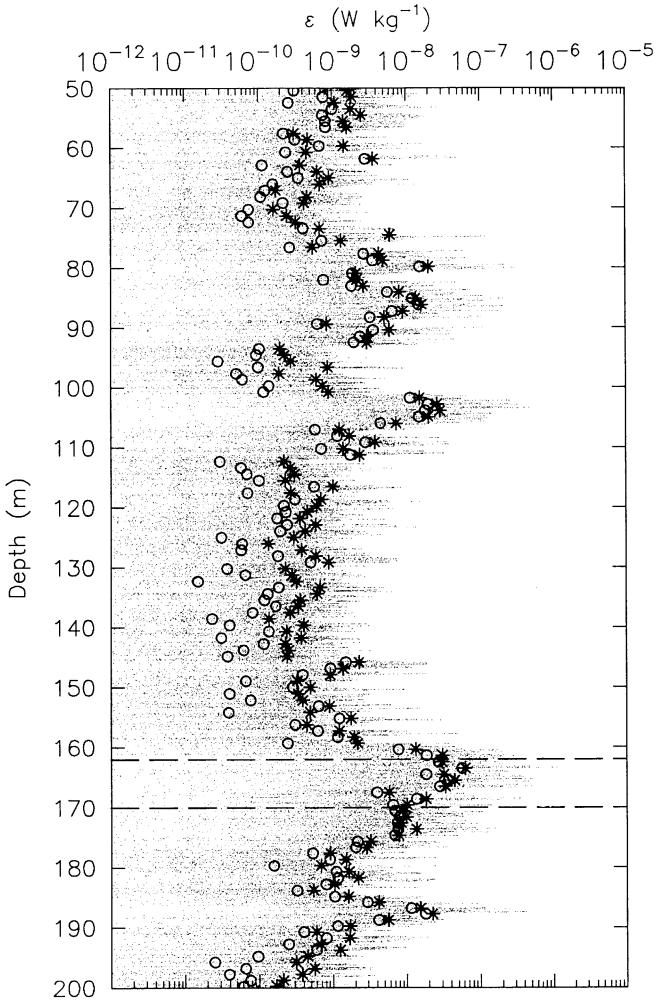

Fig. 3.9. Vertical profile of dissipation rates computed from $\partial v/\partial z$. The open circles are 1-m-average dissipation rate values computed from a conventional spectral method. The circles represent unsmoothed local dissipation data, and the asterisks represent the average local dissipation rate over 1 m. The dashed-line segment shows the 8-m segment used for the testing lognormal distribution in Fig. 3.10.

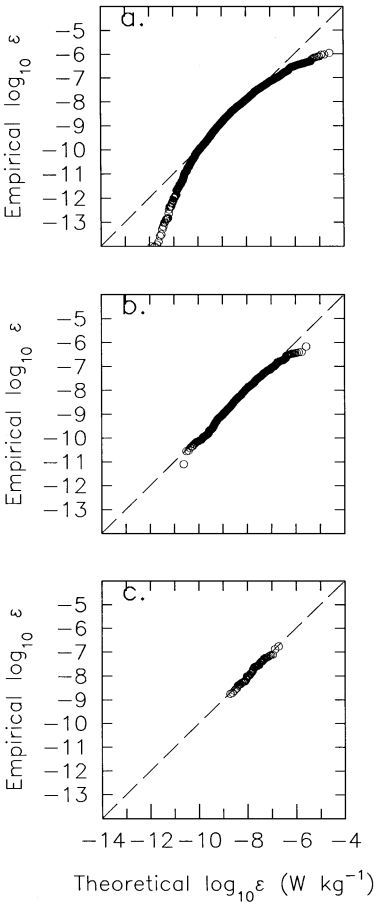

Fig. 3.10. Quantile–quantile plot of the "local" dissipation rate: (*a*) no averaging; (*b*) 5-point ($r = 3\eta$) averaging; (*c*) 64-point ($r = 40\eta$) averaging.

Numerical Simulations

How does the flow field look in 1 m^3 of water? How does a planktonic organism behave in turbulence? Field data only provide a limited aspect of the information, because field observations are usually made at a grid or along a single spatial axis and usually averaged over length scales of approximately 1 m. Therefore, at present one must make use of numerical modeling approaches to investigate the details of a microscale flow field.

Mixing is a consequence of turbulent flows, but *stirring* is part of turbulent motion, because stirring is a kinematic effect of turbulence. The theory of Rothschild and Osborn (1988) considers part of this kinematic effect—that based on an uncorrelated part of the turbulent velocity field. Yamazaki et al. (1991) confirmed their theory using a numerical model, by solving the full set of Navier–Stokes equations so that the calculated flow fields were "real." An interesting aspect revealed by this type of numerical simulation, called direct numerical simulation (DNS), is that the flow fields exhibit organized structures. One must consider both the traditional random

walk effect (uncorrelated part) and the rather new concept of coherent flow structure (correlated part) as the immediate physical environment of zooplankton (Yamazaki, 1993).

Consider a volume-averaged dissipation rate for a turbulent patch of 10^{-8} W kg^{-1}, which is a reasonable value in the thermocline. Yamazaki et al. (1991) performed a Lagrangian simulation of passive and active particles moving in a turbulent flow in an artificial cubic box with sides of length 43 cm (Fig. 3.11). The total number of time steps was 1200, equivalent to an elapsed time of 15.6 min. The rms velocity of turbulence was 0.28 cm s^{-1}, about 10 times larger than the Kolmogorov velocity scale (0.032 cm s^{-1}). The passive trajectories (Fig. 3.11*a*) exhibit the effects of small eddies. One should notice that the entire process evolves slowly but the effects of microscale eddies are clearly apparent. As we add a random walk on top of the passive particle motion, we can test the sensitivity of particle trajectory to organism behavior. With an equivalent of the Kolmogorov velocity scale, the additional random walk does not alter the trajectories (Fig. 3.11*b*), whereas 10 times the Kolmogorov scale significantly changes the trajectories (Fig. 3.11*c*). This last case is almost indistinguishable from the case of a pure random walk (Fig. 3.11*d*).

Are we obtaining a consistent picture of real turbulence with DNS? Is the lognormal theory applicable to the computed shear field from DNS? Yamazaki et al. (unpublished manuscript) have tested the applicability of the lognormal theory for both 64^3 and 94^3 grid cases. The Reynolds numbers based on the Taylor microscale are 29 and 42, respectively. Grid-level dissipation rates show the same trend with the local dissipation rate for field data (Fig. 3.12). The minimum averaging scale is between 5 and 10 times the Kolmogorov scale for lognormality to hold, so it is consistent with the field data.

Making use of the lognormal theory, one can predict the probability density function of locally averaged dissipation rate over a subdomain r^3 within the parent domain L^3. Based on both field and numerical experiments, we take the minimum averaging scale r for lognormality to be 10η. Consider two typical conditions of turbulence in the upper ocean:

1. Turbulence in the surface mixing layer

$$\begin{aligned} \langle \epsilon \rangle &= 10^{-5} \text{ W kg}^{-1} \\ L &= 10 \text{ m} \\ \eta &= 5.62 \times 10^{-4} \text{ m} \\ r &= 10\eta = 5.62 \times 10^{-3} \text{ m} \end{aligned}$$

2. A turbulent patch in the seasonal thermocline

$$\begin{aligned} \langle \epsilon \rangle &= 10^{-8} \text{ W kg}^{-1} \\ L &= 1 \text{ m} \\ \eta &= 3.16 \times 10^{-3} \text{ m} \\ r &= 10\eta = 3.16 \times 10^{-2} \text{ m} \end{aligned}$$

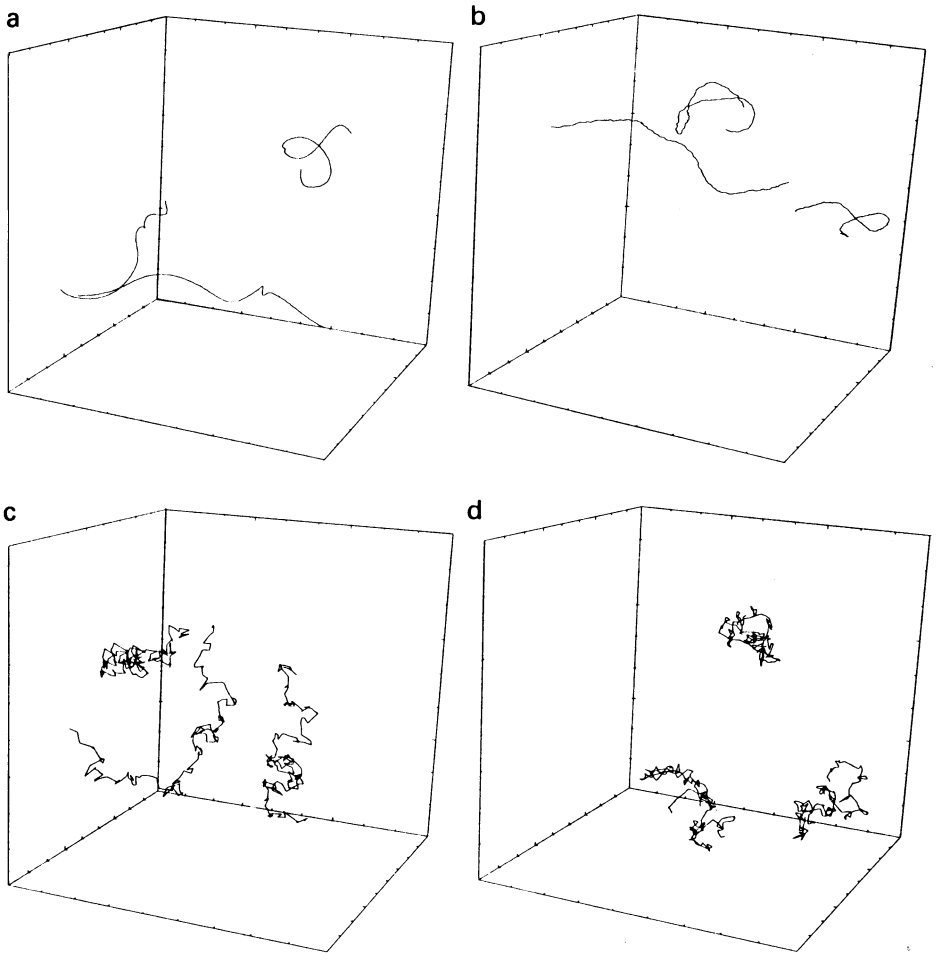

Fig. 3.11. (*a*) Three-dimensional trajectories of selected particles during the entire simulation, $T = 29.6$ (1500 steps). These particles were subjected to no random walk, so they represent trajectories of passive particles. (*b*) The same as (*a*) when random walk components whose standard deviation is Kolmogorov velocity scale are imposed on the passive particle motions. (*c*) The same as (b) with 10 times Kolmogorov velocity scale. (*d*) Three-dimensional trajectories of pure random walk particles, where the standard deviation of the Maxwell distribution is 10 times Kolmogorov velocity scale.

Since $\log \epsilon_r$ is normal, the following statistic behaves as a standard normal variable (Mood et al., 1974):

$$z = \frac{\log \epsilon_r - m_r}{\sigma_r} \tag{20}$$

When we equate $\epsilon_r = \langle \epsilon \rangle$, we find 24.8% of subdomain for the surface layer case exceeds the parent domain average, and 32.8% exceeds the corresponding parent domain average for the seasonal thermocline case. An extreme event whose average

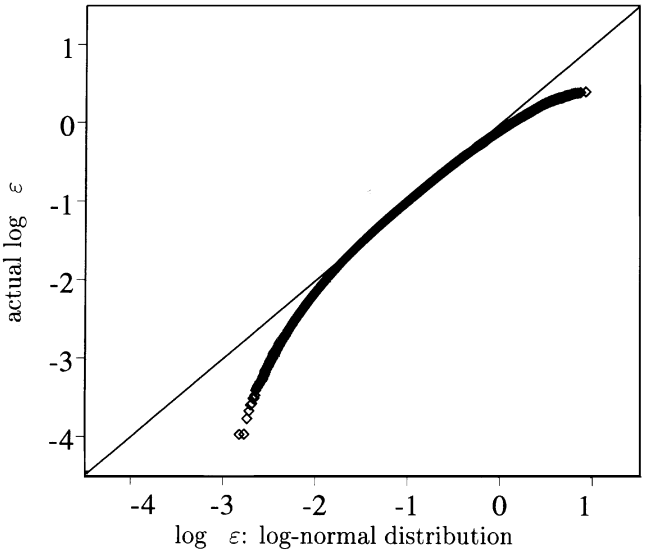

Fig. 3.12. Quantile–quantile plot of local dissipation rates computed from the DNS.

dissipation rate exceeds the significant level N^{-1} can be found from the standard normal distribution, where N is the number of subdomain cells r^3 in the parent domain L^3. For the surface mixing layer case, N^{-1} is 1.77×10^{-10}, and the corresponding value for the thermocline case is 3.17×10^{-5}. The z values are 6.27 and 3.99, respectively. Hence, the expected average dissipation rate for the two cases is 1.6×10^{-2} W kg^{-1} and 2.6×10^{-7} W kg^{-1}. If we assume the following isotropic relation for the dissipation, the expected velocity difference δu separated by a distant r can be estimated, as follows:

$$\epsilon_r \simeq 7.5\nu\overline{\left(\frac{\partial u}{\partial z}\right)^2} \approx 7.5\nu\left(\frac{\delta u}{r}\right)^2 \tag{21}$$

For the surface mixing layer case, δu is 0.259 m s^{-1}. This speed is considerably larger than the swimming speed of most zooplankton. Zooplankton cannot overcome this velocity scale. The velocity difference for the seasonal thermocline case is 0.006 m s^{-1}. This velocity scale is not so large in comparison with swimming speeds of most mesozooplankton, so they may swim freely through the turbulent environment. When we set $\epsilon_r = \langle\epsilon\rangle$, the velocity difference is 0.0065 m s^{-1} for the surface mixing layer case and 0.001 m s^{-1} for the seasonal thermocline case. Thus, even the surface mixing layer turbulence contains a substantial amount of water volume whose shear can be overcome by mesozooplankton swimming.

From these two examples we conclude that the surface mixing layer can contain a significantly high locally averaged dissipation rate at any instant in time, because our probability argument is based on a single realization. From a single realization of the seasonal thermocline, we do not find a velocity shear high enough to affect the swimming ability of mesozooplankton.

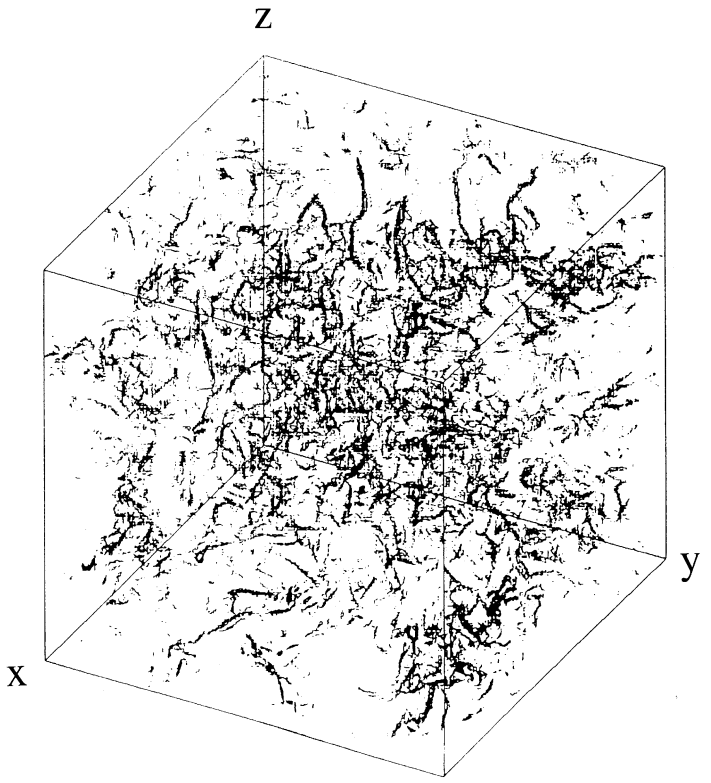

Fig. 3.13. Three-dimensional view of a vorticity field. (From Vincent and Meneguzzi, 1991; with permission from Cambridge University Press.)

Ever since the influential contribution of Taylor (1921), the conventional picture of turbulence is that of a pure diffusion process. This is still a valid concept provided that we are concerned only with the net effects of turbulence; namely, we are only looking at spatially as well as temporally averaged quantities. However, the local structure of turbulence may be more important for microorganisms than those ensemble-averaged quantities. A turbulent flow field is not random. Although one should extrapolate with caution from DNS stimulations, the numerical results provide many important aspects of turbulent flows, in particular coherent structures. Because the flow must satisfy the governing equations, locally organized flow structures tend to appear. The dominant pattern is composed of elongated thin tubes (Vincent and Meneguzzi, 1991). The width of the tubes is on the order of the Kolmogorov scale, and the length is on the order of the integral scale (Fig. 3.13). Yamazaki (1993) suggested that such an organized structure may play a significant role in a "microcosmos" ecosystem, and proposed a hypothesis: *Organized structures help plankton find mates and detect prey/predators* (Fig. 3.14). This is a difficult hypothesis to test because one must understand the details of turbulent flow structures as well as the behavior of organisms. Previous investigations (Siggia, 1981; Kerr, 1985; Vincent and Meneguzzi, 1991) show that vortex tubes are the dominant small-scale structure in many classes of turbulent flows, and numerical results show that the vorticity

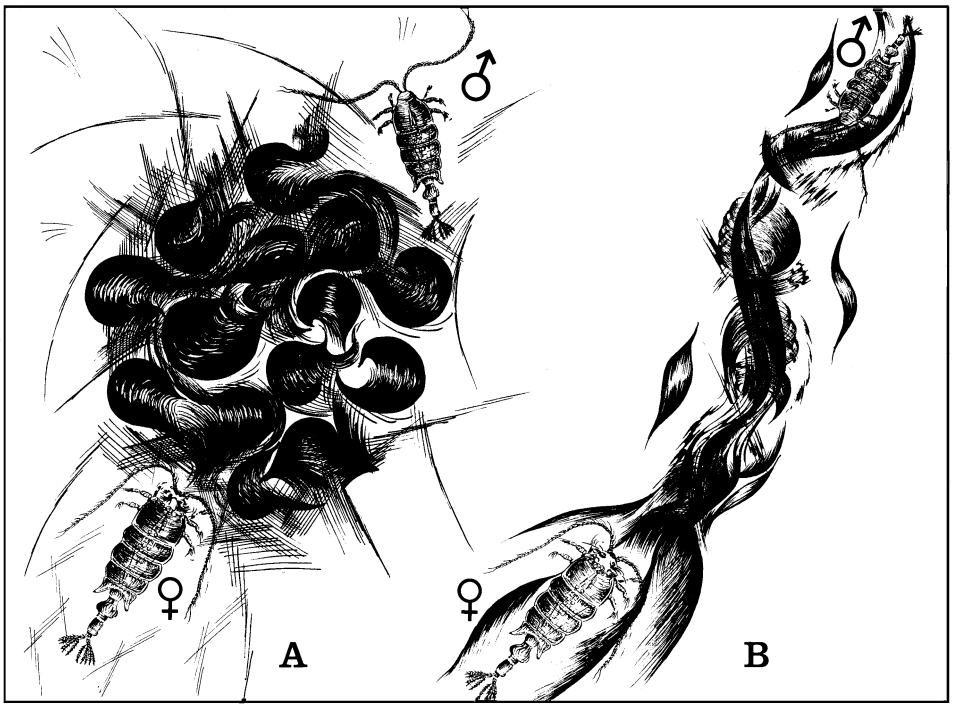

Fig. 3.14. Two hypothetical conditions where female and male plankters are searching each other in turbulence. (*A*) The flow is completely chaotic. Plankton cannot make use of flow structures as landmarks and there is no structure to help transmit messages between the two organisms. (*B*) The flow is "organized." Plankton makes use of such a structure as a landmark. The flow may help transmit messages between the two organisms.

vector, ω, is preferentially aligned with the eigenvector corresponding to the intermediate value of the strain rate tensor (Jiménez, 1992). The state of the strain field can be characterized by the quantity S^* defined in the equation

$$S^* = \frac{-3\sqrt{6}\,\alpha\beta\gamma}{(\alpha^2 + \beta^2 + \gamma^2)^{3/2}} \tag{22}$$

S^* is basically the product of three eigenvalues of the strain rate. [Kundu (1990) is a good reference for the description of velocity strain tensor and eigenvalues.] The quantities α, β, and γ are the minimum, intermediate, and maximum eigenvalues, respectively. For incompressible flow, the continuity condition requires that $\alpha + \beta + \gamma = 0$. Thus, α must be positive, γ negative, and β can be either positive or negative. The definition of S^* guarantees that it ranges between -1 and $+1$. The sign indicates that the flow is either axisymmetric expansion or contraction. The values obtained from DNS are mostly positive, indicating that isotropic turbulence has an axisymmetric expansion as a preferred strain state (Fig. 3.15).

Squires and Yamazaki (1995) performed a numerical simulation to study the effects of organized turbulent flow on marine particles using the DNS technique.

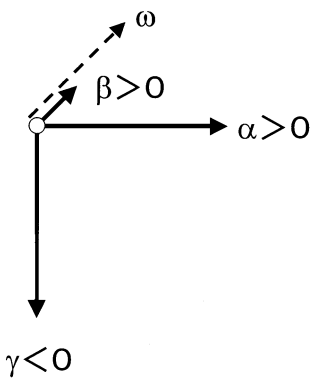

Fig. 3.15. Velocity strain at any given point (open circle) can be expressed by three eigenvectors. The corresponding eigenvalues, α, β, and γ, satisfy the continuity condition for incompressible flow; thus the sum of these values has to be zero. According to DNA studies, β tends to be positive, so the flow is expanding in the α and β directions and contracting in the γ direction. Simulations also show that the vorticity vector ω tends to align with the direction of β.

The simulated particles are slightly heavier than the water and sink at their terminal velocity. A simulated isotropic turbulent flow field was randomly seeded with 165,888 particles. The particles with terminal velocity showed a preferential concentrating tendency in low-vorticity or high-strain-rate regions, as Squires and Eaton (1991) had found for heavy particles. However, Jiménez (1997) stated that the simulated results were erroneous and the observed concentrations were transitional states. His comment is important, but may be misleading with regard to marine aggregate formation due to turbulence. The simulations were done properly, but as he points out, were not run long enough to reach steady-state concentrations. Thus Jiménez (1997) is correct for the steady-state results, but preferential concentration can occur during the transition toward steady state. Considering the natural condition in which marine particles fall through a seasonal thermocline, turbulent patches occur sporadically from time to time and from place to place. Hence falling particles are subjected to turbulent flow intermittently. Even if preferential concentration occurs transitionally, this may be enough to achieve aggregation due to the stickiness of marine particles. How transient the preferential concentrations are is not known.

3. Availability and Use of Sensory Information

In Section 1, we noted that the effects of the local environment on marine organisms can either be imposed entirely or mediated by active responses of the organism to local conditions. The difference between these two situations lies largely in whether or not the organism can both obtain and use information about local environmental conditions. These capabilities in turn depend on both the characteristics of environmental variability and the sensory and response capabilities of the organism.

3.1. Environmental Grain

The spatial and temporal structure of environmental variability (intensity, spatial extent, temporal persistence, predictability) has important consequences for how that

variability is perceived and responded to by the individual organism. About 35 years ago, Richard Levins and co-workers developed a concept of environmental grain in theoretical studies of niche selection, specialization, and genetic polymorphism. We believe that this concept will prove useful both for explaining and raising new questions about the interaction between plankton and turbulence. The theory (Levins, 1962, 1968; Levins and MacArthur, 1966; MacArthur and Pianka, 1966) suggests that animals can and should respond differently to fine-grained versus coarse-grained patchiness of their environments. The basic definitions and arguments follow.

A fine-grained environment is one in which the individual experiences/encounters the full range of differing environmental conditions in direct proportion to the relative frequencies of those conditions in the environmental continuum. This occurs because the individual cruises or drifts indiscriminately among many environmental patches spanning the full local range of conditions; it does not or cannot maintain itself within any selected portion of the environmental gradient. It therefore over time experiences and exploits the average environment. Depending on the amplitude of environmental variation, it may either exhibit generalist response or specialization on the most frequent patch phase (Levins, 1968). Conversely, in a coarse-grained environment, the individual is able to identify, select, and maintain itself within a portion of the range of environmental conditions. The animal can recognize a patch, choose to stay within it, and specialize on exploiting the conditions it finds there; in the extreme, it may spend its entire life within a single environmental patch. Over time it therefore integrates a selective subset of environmental conditions; its experience is far from a nonselective overall average.

The usual metaphor (and ecological interpretation) has been of environmental spatial grain relative to the size and motility of the organism: a bear compared with a crawling insect in a landscape that includes both forest and meadow. However, the concept applies more generally to the ability of the individual to detect and generate temporal autocorrelation of its local environmental conditions. Roughly, "fine-grained" equates to "next encounter unpredictable based on recent past experience." Note that there can be both environmental and sensory components: lack of predictability can arise either from a rapid decorrelation of the environmental field, or inability of the individual to detect and respond to autocorrelated structure present in the field.

Studies of patchiness indicate that zooplankton experience the environment as coarse-grained at spatial scales larger than a few meters in the vertical and a few hundreds of meters in the horizontal [see review by Mackas et al. (1985)]. But to what extent does the physical environment appear coarse to zooplankton at centimeter to meter scales? Spatial structure at these scales is certainly present (e.g., Yamazaki, 1993; Cowles et al., 1998; Osborn, 1998). An important characteristic and consequence of the turbulent cascade is the sharpening of small-scale gradients by the deformation and fragmentation of large-scale variance. In most upper ocean regions, the peak of the kinetic energy dissipation (i.e., velocity gradient) spectrum occurs at centimeter to decimeter length scales (Gargett, 1997). Two typical dissipation rates in the upper mixing layer and a seasonal thermocline mentioned in Section 2, namely 10^{-5} and 10^{-8} W kg^{-1}, exhibit the velocity gradient peak at 50 and 8 cpm, respectively (Fig. 3.16). Thus the length scale over which velocity gradients are in general strongest is somewhere between 1 and 10 cm. For temperature gradient spectra, the peak occurs at 300 and 50 cpm for each dissipation rate. For salt gradient spectra, the

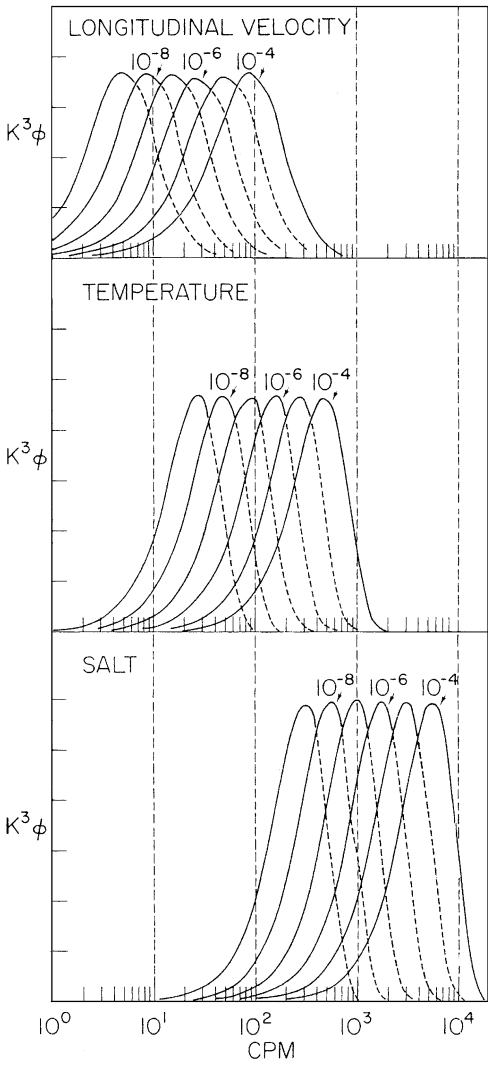

Fig. 3.16. Energy-preserving spectra for velocity, temperature, and salinity in fully turbulent flows. The Kolmogorov spectrum and Nasmyth's empirical shape for the viscous range are used for the velocity; the Batchelor spectrum is used for the scalers. Curves are plotted for ϵ varying factors of 10 between 10^{-9} and 10^{-4} W kg^{-1}. (After Gregg, 1987.)

peak takes place at 3000 and 600 cpm for each dissipation rate. Dissolved chemical signals released from zooplankton, or from their prey and predators, should behave like the salinity field, so their spatial patterns are likely to be substantially modified from the original pattern by turbulence in the upper ocean. Even in the thermocline case, an appreciable change in the chemical trace due to turbulence is expected. On the other hand, no significant turbulent velocity gradient at 1 mm scale (1000 cpm) is expected even in the upper mixing layer, although the intermittency can generate an extremely energetic spot. As noted in Section 2, the histogram of turbulence intensity versus occurrence frequency is strongly skewed when measured either along a line

in space or through time at a single location. Much of the total turbulence intensity is concentrated in few and short segments within the serial record and is therefore interpreted as strongly intermittent (e.g., Jou, 1997): burstlike in time and, at any instant, active in only a small fraction of the local fluid volume. It is less clear whether from the perspective of a plankton organism embedded in them, the small-scale gradients produced by turbulence have spatial and temporal structure that can be discerned and occupied. The alternative is that turbulence simply imposes on the organism a random and uncontrollable sequence of changing and perhaps adverse conditions. Inability of our instruments to detect autocorrelated structure is not conclusive evidence that this structure is absent. Zooplankton are smaller, and almost certainly more reactive, than any instruments that humans might use to measure turbulence. It is at small scales that we expect their sensory and behavioral attributes to be most effective: Signal contrasts (gradients) are strong, but distances are short, and much of the total velocity is shared with surrounding fluid and nearby biota. The zooplankton have sensory and behavioral reference frames that are neither Eulerian nor "frozen field," and probably also differ from the conventional "water-parcel-following" interpretation of a Lagrangian reference frame. And like most small organisms, their time axis is dilated such that a small number of seconds can contain a large number of complete and complex behavioral sequences (e.g., Strickler, 1977; Koehl and Strickler, 1981; Paffenhofer et al., 1982; Yen, 1988; Tiselius and Jonsson, 1990; Bundy et al., 1998). This time dilation means that even briefly autocorrelated local environmental structure can be interpretable and behaviorally exploitable by planktonic organisms.

3.2. Sensory Information

The sensory biology of aquatic animals (Atema et al., 1988) and, more recently, sensory ecology (Dusenbery, 1992) have become well-established disciplines within biology. However, concepts and results from these fields are only recently being recognized and applied in biological oceanography. This section includes information and speculation about how the sensory abilities and limitations of plankton affect their interactions with their small-scale physical environment.

An individual organism has diverse activities (see Table V) that it accomplishes (or attempts to accomplish) in interleaving sequence. The individual is far more likely to be successful (i.e., survive, grow, and reproduce) if the detailed timing of its activities is matched to the timing of environmental risks and opportunities. To achieve this timing match it relies on information of two sorts. Internally coded genetic information provides approximate programs for evolved developmental and behavioral strategies (e.g., annual life cycle, winter dormancy, seasonal or diel vertical migration, jump if touched). Sensory information allows an individual organism to make behavioral choices and (in some instances, physiological and developmental choices such as timing and location of larval settlement) that fine-tune its genetically programmed repertoire to fit its immediate and local experience. The animal's responses determine much of its moment-by-moment activity ("doing what") and can also affect its position ("where") at all scales larger than its own body size. The effectiveness of the responses depends both on the ability to receive and interpret information, and on the ability to respond at a scale appropriate to the environmental gradient. An individual needs accurate information about selected aspects of its environment (especially the proximity and direction to opportunities and hazards such as food, predators, mates,

and physical boundaries). What actually impinges on the animal are rapid and continuous streams of diverse scalar and vector stimuli produced by a variety of generating sources that are located at differing directions and ranges.

Dusenbery (1992) provided an extended discussion of how information content rankings can be applied to the many possible environmental signals. A brief summary follows here. Possible stimuli include temperature, gravity, light, other electrical and magnetic fields, chemicals, the spectrum of high-to-low frequency vibration (sound and mechanical displacement), and mechanical contact. For signals that do not involve direct contact of recipient with source, possible modes of through-water transmission include radiation (light and vibration), diffusion (chemical), and flow (shear and transport). Out of the potential range of signals, most organisms pay significant attention to only one or a few to cue any particular response, partly because of differential effectiveness, and partly for metabolic, neural, and structural parsimony. How well a given mode of input can be received and interpreted is affected by factors such as strength-at-source, transmission properties of the signal channel (usually, the intervening water), presence and strength of masking noise, sensitivity and directionality of sensory receptors, and subsequent internal processing by the nervous system of the receiving animal. These factors exert a strong selective pressure on what kinds of environmental stimuli are used for what purposes. An environmental signal is most useful if it combines strength (relative to noise), detectability (relative to sensor threshold), specificity (relative to signals from qualitatively different sources, e.g., predator versus mate), and directionality.

Knowledge of the structure and capabilities of zooplankton sensory systems has grown enormously during the 1990s, especially for small crustaceans and medusae [e.g., the symposium proceedings edited by Lenz et al. (1996a)]. Assuming that evolution has in general selected for "what works best," this new information allows many interesting deductions and speculations about how plankton extract information from and subsequently react to their local environments.

- Many (probably most) zooplankton have extensive arrays of external mechano- and chemosensory receptors (Friedman, 1980; Gill, 1986; Yen and Nicoll, 1990).
- Both mechanoreceptors and chemoreceptors are concentrated in particular locations on the surface of the animal that maximize their utility. For example, many copepods have long first antennas that project laterally from their heads. The mechanoreceptive setae that detect fluid shear are especially prominent along and near the tips of these antennas (Yen and Nicoll, 1990; Fig. 3.17). These setae are extremely sensitive to flexion by local shear, such as might be generated by motions of a nearby predator or prey item (Yen et al., 1992; Bundy et al., 1998). Their distal locations serve both to isolate the sensors from disturbances generated by the animal's own midbody swimming appendages, and perhaps to maximize sensitivity to particular vibration frequencies and to provide a large separation baseline for resolving signal directionality (Yen and Nicoll, 1990).
- Chemoreceptors are believed to be important for finding/selecting both food (Koehl and Strickler, 1981; Poulet and Ouellet, 1982; Cowles et al., 1988), forming aggregations (Poulet and Ouellet, 1982), and locating mates [papers in Boxshall (1998)]. Planktonic shrimps follow rapidly and accurately the scent trails left by sinking food particles (Hamner and Hamner, 1977). Copepods

chemoreceptors are abundant both on the antennas (Lenz et al., 1996b) and in the vicinity of the mouthparts (Friedman, 1980).

- Although many zooplankton continue to be termed *filter feeders*, it is now clear from many studies that the process of finding and selecting food items often involves sensory detection and specific behavioral responses, and is not in general simply a sieving of food items from a steady feeding current.
- For food location and discrimination, the relative importance of different receptor locations (e.g., antennas versus mouthparts), of mechano- versus chemoreception, and of long- versus short-range or contact reception is still somewhat unclear (DeMott and Watson, 1991; Bundy et al., 1998; Frey et al., 1998; Yen et al., 1998). Differences in feeding and predator avoidance strategy may be important, as well as overall body morphology. For example, the flow streamlines of feeding currents generated by suspension-feeding copepods are most intense near, and directed toward, the copepods' mouthparts; little or no feeding current flow crosses their antennas (Bundy, personal communication; Strickler, 1985; Tiselius and Jonsson, 1990; Bundy and Paffenhoffer, 1996).
- Light sensors are present in some zooplankton taxa but are less prevalent and less sophisticated than in larger vertebrate and cephalopod taxa. It has been known for several decades that light reception plays a strong role in controlling zooplankton vertical migration behavior and that stimulated light emission (bioluminescence) is for some taxa an important aid to predator avoidance and/or mate recognition. Newer research is demonstrating the importance of small-scale variability in light intensity as a cue mediating small-scale swarming (Buskey et al., 1996).
- Internal sensors of acceleration (e.g., the statocysts used by decapod crustaceans and cephalopods to detect both gravity and angular acceleration) are rare or absent in the smaller zooplankton (Budelmann, 1988). Rather than direct sensing of the gravitational vector, zooplankton appear to maintain directional orientation by a combination of light cues, a balancing of drag and buoyancy forces (Strickler, 1982), and perhaps detection of shear differentials between different parts of their body surfaces.

Small-scale water motions affect in various ways the strength and quality of pelagic environmental signals and the ability of planktonic organisms to detect and interpret them. For scalar tracers such as temperature and dissolved chemicals, small-scale advection alters the spatial distribution of the signal and thereby affects its strength and directionality. In particular, small-scale water motions deform and steepen the local signal-strength gradients. This deformation and steepening can have important consequences for the ability of a small organism to track a signal back to a far-field source location (i.e., distant by several to many meters)—the local upgradient direction may have little or no vector correlation with the large-scale flow and may lack continuity if turbulent deformations produce small and transient "islands" of high local signal level. The turbulent steepening of gradients also increases the rate at which signals are attenuated over time by molecular diffusion, conductivity, and/or chemical reactivity.

For fluid mechanical signals such as shear, acceleration, and vibration (such as might be produced by an approaching predator or mate), small-scale water motions add particularly complex and interesting effects (Kiorboe, 1997). For this class of

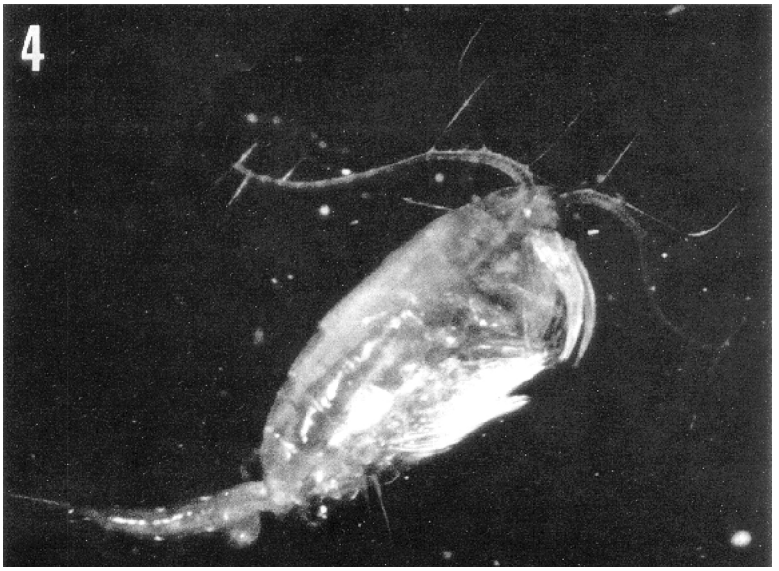

Fig. 3.17. Mechanosensory setae on the antennas of the copepod *Euchaeta norvegica.* Placement on the long antennas allows the setae to extend into relatively undisturbed water. Three-dimensional orientation of the setae [see Yen and Nicoll (1990) for views from additional perspectives] probably allows directional discrimination. (From Yen and Nicoll, 1990, Copyright 1990, The Crustacean Society.)

sensory information, biological/environmental signal and turbulent "noise" are likely to be received and interpreted by the same sensory apparatus (e.g., bending or tilting of individual appendages and setae, or tumbling and rotation of the entire organism relative to gravity or illumination fields). As noted in Sections 4.1 and 4.3, the cost of failing to sense and respond to close proximity of a predator is potentially very high (immediate risk of death), so plankton organisms make large morphological investment in predator detection. Fluid disturbance commonly elicits cessation of normal feeding and swimming activity and one or another defence response (flight or "playing possum"). An important point is that small-scale eddies and vorticities can generate small-scale gradients; they can in themselves be signals if varying over scales equal to or smaller than the organism.

4. Coupling to Biology

4.1. Selective Pressures

Individual-level biological processes affected by the small-scale physical environment influde feeding, predator avoidance, aggregation, and mating. Within the life span of any individual organism, realizations of these processes take place as a sequence of more-or-less discrete biological events and activities (Table V). Individuals differ, both by chance and by genetic endowment, in the methods and success with which they deal with the challenges presented by each event. Evolutionary selection increases the frequency of those genetically controlled somatic traits, life history patterns, and behaviors that enable the organism to complete all steps successfully. We therefore observe in the present a preponderance of those traits and environmen-

TABLE V
Examples of Life Cycle Events Affected by the Small-Scale Physical Environment

Life History Event	Urgency	Frequency of Repetition
Life stage transitions (hatching, metamorphosis, settlement, migration)	Low to acute	Episodic, usually one to several per life cycle
Foraging	Chronic need, but becomes progressively more acute with past lack of success	Frequent, usually several to many per day
Predator avoidance	Acute (failure means death)	Rare to frequent, depending on prey–predator combination
Mating and reproduction	Minor for individual survival but essential for production of offspring, hence strong evolutionary selection for individual investment	Single or repetitive; often concentrated late in the individual life span

tal adaptations that have worked well in the past. The adaptive fitness of a given organism or trait (strictly of its genotype) is defined and indexed by the degree to which the expected number of reproductively viable offspring is maximized. Because this can be difficult to observe, interim goals such as maximization of food intake, growth rate, or fecundity are often used as proxy indices of adaptive fitness.

An extensive ecological literature has analyzed both evolutionary process and adaptive outcome as a game theory optimization problem. For a general introduction to this approach, see Maynard Smith (1992); for some applications specific to zooplankton ecology, see Kerfoot (1980). The following brief summary points will be relevant to our discussion:

- The various events that make up the life sequence differ in their urgency (acute versus chronic need), timing, and frequency of recurrence (Table V). They also interleave and interrupt each other. When they do so, our expectation is that behavioral responses to needs or risks that are both immediate and extreme (e.g., predator avoidance) will override less urgent "postpone-able" behavior (e.g., continued feeding by a well-nourished individual).
- Prey detection (discussed in Section 4.2), predator avoidance (Section 4.3), and mate location (Section 4.4) activities all dependent on the animal's ability to obtain and interpret sensory information about the identity, direction, and proximity of surrounding organisms. The surrounding small-scale physical environment can degrade this ability in two ways. One is a transmission path effect: distortion and attenuation of "real" signals generated by surrounding organisms. The second is by physical generation of noise that masks or mimics the biologically generated signals, leading to ineffective or inappropriate response.
- Within some of the event classes shown in Table V, there are likely to be several alternative modes of risk and benefit, with associated trade-offs for any particular behavioral or developmental strategy. For example, an organism usually has access to more than one food source and is vulnerable to being killed by several very different types of predator.
- Optimality is a shifting target that depends critically on environmental context.

Over relatively long time scales, this causes new species to appear and old species to go extinct. Over shorter time scales it can produce real or apparent mismatches to present conditions: for example, compromise bet-hedging strategies that are robust over a broader range of environmental variability, or "evolutionary arms races" between predator–prey or competitor pairs.

- Slightly less obvious, optimality is also affected by fluctuations in the condition, recent history, and/or life stage of the individual organism and may often be achieved by a range of situational responses (dynamic optimization: Werner and Gilliam, 1984; Mangel and Clark, 1986; Clark and Levy, 1988). One example: a starving animal (which will die anyway if it does not obtain food) can be expected to accept more predation exposure (risk) to obtain food (benefit) than a satiated animal.

4.2. Feeding

Much of the intial and present interest in the interaction between turbulence and marine organisms has focussed on the effects of turbulence on zooplankton and larval fish feeding rates. The reviews by Dower et al. (1997) and Alcaraz (1997) and other papers in Marrasé et al. (1997) provide good summaries of progress through the mid-1990s. In this chapter we briefly summarize some of the main ideas and then review a few newer results.

The present understanding of how small-scale physical and biological processes and their associated constraints affect these steps has come mainly from two approaches: laboratory cinematographic observations and mathematical models. A common approach in both theoretical and observational analyses of feeding activity is to decompose each feeding event into sequential steps (e.g., Gerritsen and Strickler, 1977): (1) searching (leading to encounter), (2) pursuit and capture, (3) postcapture handling, and (4) ingestion. Typical assumptions in this analysis are that all steps must be completed for the feeding process to be successful, that completion of each step leads to initiation of the subsequent step, that failure at any stage causes the predator to revert back to the start of the sequence, and that total feeding rate is limited by time competition among these (and possibly additional) activities.

Visual and high-speed cinematographic observations, initially of tethered zooplankton (e.g., Koehl and Strickler, 1981; Paffenhofer et al., 1982) and more recently of zooplankton and fish larvae swimming freely in aquaria (e.g., Tiselius and Jonsson, 1990; MacKenzie and Kiorboe, 1995; Bundy and Paffenhofer, 1996; Bundy et al., 1998) have demonstrated that planktonic predators (even those classed as filter feeders):

1. Detect their prey at distances of order one or more body lengths, using either or both chemical (e.g., Poulet and Ouellet, 1982) and mechanical (e.g., Bundy et al., 1998) signals.
2. Execute rapid and relatively complex behavioral sequences of pursuit and/or flow diversion that, if successful, capture the prey item.
3. After capture, execute additional inspection and handling behaviors. Strickler (personal communication) also shows that the animal can differentiate nonedible food from edible food.

Observations that all of the above are often completed within a fraction of a second show clearly that the animal is well equipped and programmed to find and handle its food, and that its perceptual and response time scales are very rapid. An important and not-yet-fully-answered question is if and how these laboratory-demonstrated food-gathering capabilities are enhanced or degraded in the ocean environment. Two characteristics of the open ocean situation are likely to be important: (1) the presence of physically imposed small-scale flows (turbulence) and (2) the ability of the free-swimming animal to move through and perhaps select its local environment.

Is feeding rate affected by the imposed intensity of turbulence? Many theoretical and observational studies now indicate that the answer is a qualified yes. The historical starting point for this line of inquiry was a theoretical analysis by Rothschild and Osborn (1988), who showed that turbulence increases the encounter rate between prey and predator. The basis for the encounter-rate-enhancement theory is that turbulent shear produces a velocity difference between water parcels containing prey and predator that is in addition to the swimming velocities of prey and predator. This differential motion increases the frequency with which the predator and new prey items come close to each other. Various differently formulated mathematical models have repeated this conclusion [e.g., references cited by Dower et al. (1997) and Alcaraz (1997)], as have laboratory and field observations of time-integrated feeding and growth rates [see review by Dower et al. (1997)]. The enhancement is dependent on body size and separation scale both because of trends with body size in swimming speed and sensory detection range, and because of the scale dependence of turbulent velocity. The latter point is important because as the separation distance between two water parcels gets smaller, the parcels share the same eddy structure to a greater and greater degree. Turbulent velocity differences therefore decrease, because the total turbulent velocities of the two parcels are progressively more correlated. Choice of length scale for prey–predator interaction therefore has a large effect on calculated encounter rate enhancement. However, despite extensive experimental and theoretical research, there remains disagreement in the literature about which spatial scale to use: perceptive radius versus mean prey–predator separation distance [compare, e.g., Kiorboe and MacKenzie (1995), Incze et al. (1996), Kiorboe (1997), and Sundby (1997)]. Because perceptive radius is almost always much smaller than mean separation distance, the former choice (which we believe is correct) reduces the predicted encounter rate enhancement by factors of 2 or more.

A clear observational test for encounter rate enhancement is possible for animals such as fish larvae that assume recognizable "attack" postures when they detect prey items. Using this approach, MacKenzie and Kiorboe (1995) compared effects of turbulent ($\epsilon = 7.4 \times 10^{-8}$ W kg^{-1}) vesus calm surroundings on fish larvae with cruise (herring) versus pause–travel (cod) visual search strategies. They found that turbulence increased the encounter rate for both search strategies at prey concentrations less than about 50 nauplii per liter, but that the relative enhancement was greater for the pause–travel strategy than for the continuous-cruising strategy (Fig. 3.18). In a parallel theoretical analysis, Kiorboe and Saiz (1995) examined effects of predator motility and search strategy on the Rothschild and Osborn (1988) and similar models of encounter rate enhancement. They approximated the effects of relative motion between prey and predator on encounter rate as the sum of two components, one due to behavioral motion and a second due to turbulence. Kiorboe and Saiz (1995) concluded that proportionate enhancement is greatest for predators with body size in

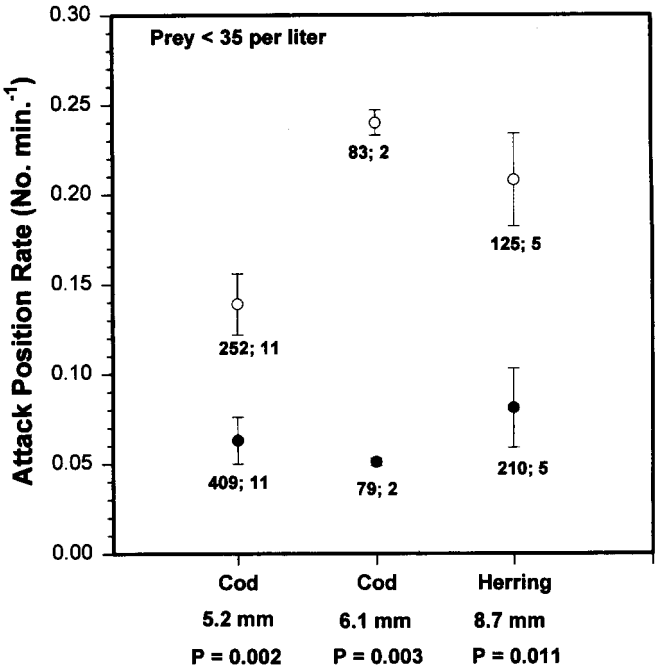

Fig. 3.18. Comparison of prey encounter rate (indexed by frequency of "attack position") for cod and herring larvae in calm (filled circles) and turbulent (open circles) laboratory enclosures. Unsatiated larvae assume a recognizable attack posture when they become aware of a nearby prey item. At low to moderate prey densities, the turbulent encounter rate is higher for both pause–travel (cod) and continuous-cruising (herring) search strategies. (From MacKenzie and Kiorboe, 1995.)

the millimeter to centimeter range and with long prey-detection distances. Of various search strategies, they conclude that enhancement is greatest for stationary ambush predators, intermediate for cruising predators, and least for predators that rely on scanning of a self-generated feeding current.

Turbulence also affects the postencounter steps in the food-capture sequence [see Alcaraz (1997) for a more detailed review of this topic]. Several observational studies on tethered or confined animals have shown that zooplankton behavioral patterns differ in still-water versus imposed turbulent conditions (Costello et al., 1990; Marrasé et al., 1990; Saiz and Alcaraz, 1992), often involving an increase in swimming speed and frequency of escape responses. Costs of this behavior include both increased metabolic demand (see Alcaraz, 1997) and some disruption of time spent in normal food-seeking behavior. In addition, the same turbulent velocity differentials that enhance encounter rate may conversely make pursuit and capture of detected food items less effective, leading to a decline at high turbulence levels in the efficiency with which encounters are converted to captures and therefore to a dome-shaped curve of feeding rate versus turbulence intensity (MacKenzie et al., 1994; Fig. 3.19).

All of the arguments above about feeding rate assume that plankton and larval fish experience turbulence intensity as fine-grained (Section 3.1): that the turbulent velocities that they will experience have the same intensity and duration statistics as a random sampling of their local environment. Behavioral and sensory capabilities of

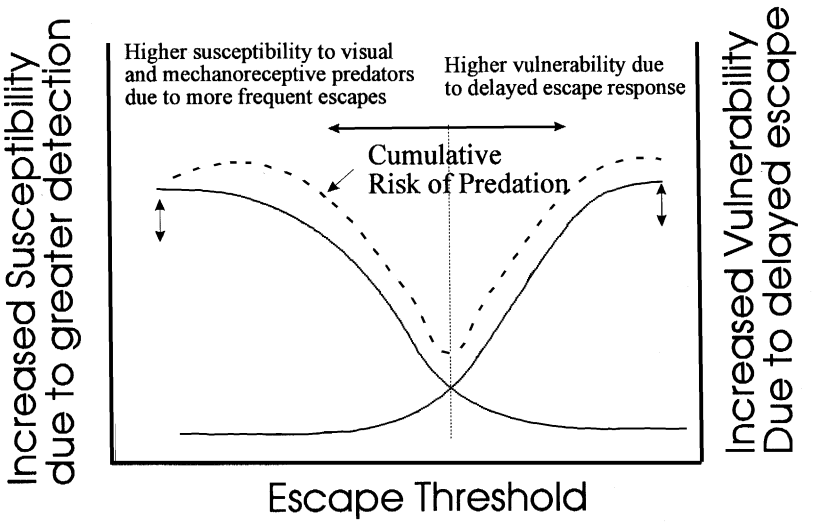

(*a*)

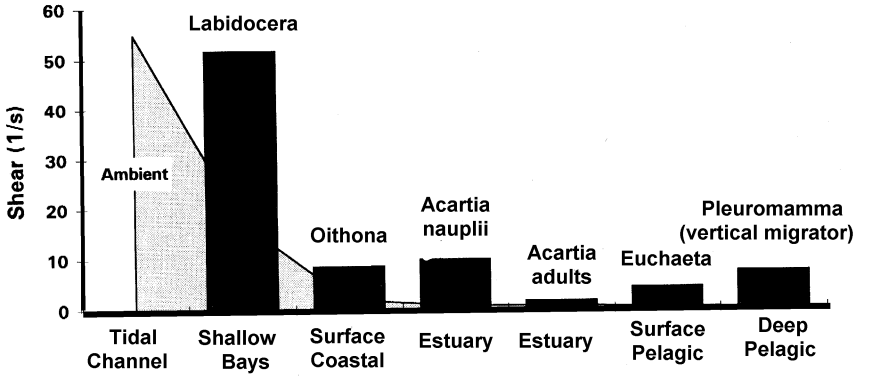

(*b*)

Fig. 3.19. (*a*) Optimum escape threshold is a balance between risk of delayed escape versus false alarm escape response. (*b*) Species dependence of escape response threshold appears to be correlated with ambient shear rates in the species' normal ocean habitat. (From Fields and Yen, 1997. Reproduced by permission of Oxford University Press.)

zooplankton and larval fish may make this assumption invalid both at macroscopic (meters to tens of meters) and microscopic (millimeter to tens of centimeters) scales. At the macroscopic scale, field observations have consistently shown strong vertical layering of both plankton and larval fish abundance and turbulence intensity (Figs. 3.5 to 3.7). Order-of-magnitude changes both in concentration and in turbulent dissipation rate are relatively common across vertical distances of 1 to 10 m, sometimes even less. Directed vertical swimming at speeds of order cm s^{-1} can therefore substantially change the turbulence characteristics of an animal's local environment if

the vertical swimming is sustained or repeated for a few tens to hundreds of seconds. Plankton and larval fish are easily capable of making these vertical excursions, and many do so in response to diel changes in light intensity. How often similar changes in vertical position are carried out in response to turbulence cues is less certain at present. However, there is evidence showing that vertical distribution of plankton is correlated with the vertical distribution of turbulent shear.

Mackas et al. (1993) found evidence that vertical distributions of the dominant North Pacific upper ocean copepods follow "preferred" levels of turbulence over time scales of hours to days, with some taxa moving away from the surface during time periods of strong wind mixing, while others remain aggregated in the turbulent mixing layer. In U.S. GLOBEC studies near Georges Bank, Gallager et al. (1996) found that *Calanus finmarchicus* aggregated at sites and depths where the gradient Richardson number Ri was large (combination of high static stability and low vertical velocity shear), and Incze et al. (1996) found aggregations of nauplii associated with the most strongly stratified sites and depth strata. Numerous behavioral and neurophysiological studies have demonstrated response by crustacean zooplankton to bending of their mechanoreceptory setae (see Section 3.2); the velocity gradients responsible for this bending can be generated either by other nearby organisms (prey, predators, mates depending on the situation) or by small-scale turbulence.

At the microscopic scale, full numerical simulations of turbulence DNS shows that the nonlinear process of turbulence generates small-scale vortex tubes that persist for durations of order seconds to minutes (see Section 2.2; see also Vincent and Meneguzzi, 1991; Yamazaki, 1993). Vorticity and strain components are directionally correlated within these structures, and cross-section scales are comparable to body sizes of the larger zooplankton. It is therefore possible that zooplankton can detect and orient themselves relative to these structures by direction and intensity comparisons of signals from sensors on different parts of their body surface. This behavior in turn raises the possibility that the local fluid environment is not randomly and unpredictably variable, but instead that it is, albeit continually changing, an interpretable fluid-scape well supplied with signs and route markers (Fig. 3.14). Interpretability can significantly increase the particle contact rate if the animal uses "intelligent" tactics to find either prey aggregations or clear sensory trails leading to prey items. At present, the best evidence that zooplankton do make use of such small-scale velocity gradient structures (or their chemically delineated remnants; see Hamner and Hamner, 1977) is provided by recent observations of mate-tracking behavior (described in Section 4.5).

4.3. Predator Avoidance

Each encounter with a predator is potentially lethal. This fact produces a strong evolutionary selection on prey species for detection and effective behavioral response to "signals" from their predators (Krebs and Davies, 1981). Because of the high cost of failure, prey avoidance response to predator signals should override most other stimuli and responses, such as proximity of their own prey or mates; "a predator can afford to make mistakes whereas the prey cannot" (Hamner, 1985). We also expect the selective pressure to be most intense for response to signals from dominant predator types. Predators differ both in their relative importance and in the types of signals they generate (Table VI).

TABLE VI
Alternative Modes of Predation to Which Small Zooplankton Are Exposed

Mode of Predation	Example of Predator	Predator-Prey Length Ratio	Fraction of Total Mortality	Types of Signal Generated by Predator	Comments
Short-range visual	Larval fish	10^1–10^2	Small	Along-streamline velocity gradient $\partial u_i/\partial x_i$ during approach and attack (e.g., Viitasalo et al., 1998)	Escape response make prey more conspicuous (e.g., Yen and Strickler, 1996)
Medium-range visual	Juvenile/adult fish	10^2–10^4	Moderate to large	Mechanosensory and/or visual during approach and attack; possible background chemosensory (e.g., Bollens et al., 1994)	Dominant detection mode may vary greatly among prey taxa (Bollens et al., 1994)
Ambush	Chaetognath some larval fish	5–20	Often large	Along-axis velocity gradient $\partial u_i/\partial x_i$ during approach and attack	Only predator signal is after initiation of attack event, escape response likely to make prey more conspicuous
Cruising	Euchaeta, some larval fish	0.5–5	Moderate to large	Multiaxis velocity gradients (both $\partial u_i/\partial x_i$ and $\partial u_i/\partial x_j$), during both search and attack modes of predator activity	Predator signal is also small scale; frequency, content, and rhythmicity of signal may be an important aid to signal detection and discrimination (e.g., Bleckmann et al., 1991)
Entanglement	Ctenophore, medusa	10^2–10^4	Moderate to very large	For medusae, swimming motions generate strong velocity gradients during bell contraction, much weaker flow (normal to the tentacles) during the recovery stroke (Costello and Colin, 1994)	Tentacles camouflaged by deformation along flow?

Much of the most recent (1990s) research on predator avoidance by zooplankton has been on the sensory ecology and escape behavior of copepods and cladocerans. Several studies have shown that freshwater cladocerans change their vertical distribution in response to chemicals emitted by their predators [see Folt and Burns (1999) for a more complete summary]. For copepods, hydrodynamic cues received by surface mechanoreceptors appear to be the most important method used for detecting nearby predators (Bollens et al., 1994), although chemical and visual cues may also be used. Studies of the mechanoreceptive setae on copepod antennas (e.g., Yen et al., 1992; Hartline et al., 1996; Davis et al., 1999) have demonstrated rapid, sensitive, and directional neural response to displacements of the setal tip relative to the antenna (neural response thresholds <10 nm for displacement, 20 μm s^{-1} for displacement rate). The morphology of sensor placement appears to enhance both sensitivity and directionality (e.g., Gill and Crisp, 1985; Yen and Nicoll, 1990): location near the distal tips of the antennae extends sensors as far as possible into the surrounding fluid and as far as possible away from the individual's own centers of mass and drag and any disturbances created by beating of its own swimming and feeding appendages (see Fig. 3.17).

The directionality and displacement rate dependence of the neural response suggest (Yen et al., 1992) that copepod sensory setae are used to detect velocity variation (transient movement of some or all the surrounding water relative to the copepod). But what sorts of velocity variation provide the best target signals or predator proximity, and what sorts generate behavioral responses? This question has been addressed by recent theory and experiments on individual behavioral response thresholds, and how these thresholds covary with prey and predator characteristics and with local physical environmental conditions, especially by Yen and co-workers (Yen and Fields, 1992; Fields and Yen, 1996, 1997; Yen and Strickler, 1996) and Kiorboe and co-workers (Viitasalo et al., 1998; Kiorboe and Visser, 1999; Kiorboe et al., 1999). In most of this work, the copepod is interpreted as a nearly rigid body embedded in a viscous fluid. Bending of mechanosensory setae located at the distal ends of this rigid body will result from any of several modes of differential motion, including acceleration of the copepod relative to its surroundings, a velocity gradient of the surrounding fluid along the local velocity vector (strain deformation), or a velocity gradient of the fluid across the local velocity vector (shear = vorticity, leading to both rotation and deformation). However, these modes differ substantially in how the directionality of setal bending is distributed over the surface of the animal. The nature and source of the flow disturbance might therefore be discriminated on this basis. Fields and Yen (1996, 1997) observed response distance and location relative to the flow field generated by a siphon suction tube and reported threshold shear values (for different species) ranging from about 1 to 50 s^{-1}. However, Kiorboe et al. (1999) used a more diverse range of experimental chambers (oscillating chamber, rotating cylinder, and couette tube, in addition to siphon flow) and concluded that response to strain deformation (threshold 0.5 to 5 s^{-1}) is far more sensitive than response to rotation or spatially uniform acceleration. Strain deformation is normally present in a cross-streamline sheared flow but is also present for along-streamline acceleration, such as accompanies head-on approach by an attacking larval fish (Kiorboe and Visser, 1999). Some of the present differences in interpretation may be resolved by more complete and careful three-dimensional definition and discrimination of velocity gradient vectors (e.g., Kiorboe et al., 1999; see also Section 2.2).

Response thresholds covary within species with age and body size. Older (larger) developmental stages of *Acartia tonsa* have a sixfold lower response threshold than younger stages (Fields and Yen, 1997; Kiorboe et al., 1999), probably because their larger body size allows differencing of velocity gradients across a longer spatial baseline, leading to stronger setal bending for a given velocity gradient. Numerous field population studies have shown that within-species copepod mortality rates decline with developmental stage. The sensory-threshold observations raise the interesting hypothesis that this decline is caused by improvement with age of predator detection capability as well as or instead of increase with age of prey escape velocity.

Response thresholds differ even more (order 20-fold) among copepod species (Fields and Yen, 1997). Some of this difference may be due to genetically imposed limitations in sensor capability, some may be due to species-dependent differences in swimming and orientation behavior (e.g., a copepod species such as *Neocalanus cristatus* that spends most of its time suspended vertically in the water may be more sensitive to rotational perturbation than a species that cruises with no consistently preferred orientation), and much may be adaptive to particular physical environmental conditions or suites of predators. For example, Fields and Yen (1997) found that response thresholds of copepods from estuarine versus oceanic and surface versus deep ocean environments are roughly correlated with expected ambient rates of physically generated shear in these environments (Fig. 3.19). At least two factors might select for matching or response threshold to physically generated environmental noise level. First, excessively sensitive "false alarm" high-energy escape responses are energetically wasteful for the copepod and divert it from productive activities such as feeding and mating. Second, and perhaps more important, false alarm responses are risky because rapid movements make the escaping copepod more conspicuous, increasing the detection radius for both visual and mechanoreceptive predators (Yen and Strickler, 1996). Observed response thresholds may therefore represent the evolutionary trade-off between the need to avoid "attacking" predators and the need to avoid alerting "searching" predators (Fig. 3 from Fields and Yen, 1997).

4.4. Aggregation

Abundance of planktonic organisms is spatially variable (patchy) over a wide range of spatial scales. The formation and maintenance of this variability against eventual homogenization by mixing requires spatial gradients in the local rate of change N' of abundance N (Denman, 1984). At any given spatial scale Δx, the dominant variance-generating processes are those for which the time integral of $\Delta N'/\Delta x$ over the life span of the patch is largest [see Mackas et al. (1985) and Pinel-Alloul (1995) for more extensive discussions of scale dependence]. At the largest scales, an obvious mechanism for generating spatial variability is the cumulative effect of sustained and spatially autocorrelated variation of population growth rate.

At intermediate to small scales, variations of transport and behavior, leading to localized convergence of particle trajectories, are more likely to be dominant. At patch scales smaller than a few meters, spatial variations in swimming behavior (linked to spatial or temporal gradients of various sensory stimuli) are almost certainly the most important patch generating mechanisms [see review by Folt and Burns (1999)]. In at least some instances, aggregation may involve a sequence of progressively finer scale responses to a sequence of progressively finer scale environmental

gradients. For example, the reaction distance of copepods to mechanical stimuli is roughly two to four body lengths. Haury and Yamazaki (1995) noted that nearest-neighbor distances based on observed local average abundance are usually much larger than this individual perception distance. Initial stages of aggregation probably use other cues and responses: for example, shared behavioral response to coarser scale physical and chemical variability. Once animals are sufficiently close together, they can shift to more proximate and specific individually generated signals.

It is difficult to measure planktonic distribution at submeter scales in the natural environment, but several recent developments in sampling methodology have greatly enhanced knowledge of the prevalence and characteristics of microscale plankton patchiness [see Folt and Burns (1999) for a more complete discussion]. Some examples video plankton recorder (e.g., Davis et al., 1992) and dark-field in situ video (Tiselius, 1998) observations of zooplankton abundance and orientation in patches with length scale <1 m; acoustic measurements of high concentrations of multiple species in depth strata <0.5 m thick (Holliday et al., 1998); and centimeter-scale chlorophyll variability revealed by an in situ optical imaging system (Jaffe et al., 1998) and by high-resolution profiling instruments (Cowles et al., 1998; Hanson and Donaghay, 1998). Laboratory experiments (Tiselius, 1992; Saiz et al., 1993) have demonstrated that zooplankton respond to phytoplankton patches a few centimeters in size. All these findings from both field and laboratory studies indicate that the microscale distribution of the planktonic ecosystem requires much attention in order to understand how the building blocks of the entire oceanic ecosystem works. These studies must include physical measurements at appropriate scales, because the distribution of planktonic organisms is closely tied to small-scale fluid motions.

4.5. Mating

The process of locating and getting close to a prospective mate can usefully be viewed as a special case of aggregation formation. Although a less frequent and perhaps less urgent activity than feeding or predator avoidance (see Table V), mating is for most species an essential prerequisite of reproduction and life-cycle completion. Especially for rarer taxa, average concentrations of appropriate (same species, opposite sex, mature and receptive) target individuals are very dilute. Strickler (1998) noted that "the average distance between potential mates may be too great (meters to tens of meters) for these millimeter-scale animals, swimming in random directions at millimeters per second, to encounter each other within the temporal window of sexual receptivity." It is therefore clear that mate-search activity cannot proceed in random fashion. Finding and moving close to a prospective mate is likely to be a more difficult search procedure and require more sensory discrimination than the feeding or generalized aggregation processes discussed in Sections 4.2 to 4.4.

Strickler (1998) observed a mating event of cyclopoid copepods in a 5-L container. Detailed swimming paths from male and female were reconstructed from high-speed cinematography (Fig. 3.20). Initially, the male was separated from the female by more than 10 mm. After 10 s, the male approached the female to within 2 to 3 mm, and maintained that distance for almost 20 s. The final leap took place shortly after an elapsed time of 30 s. The mating took less than 1 s. During the 20-s tracking period the male showed a synchronized swimming pattern, with his swimming speed matched to that of the female. Strickler's observations that revealed these interesting

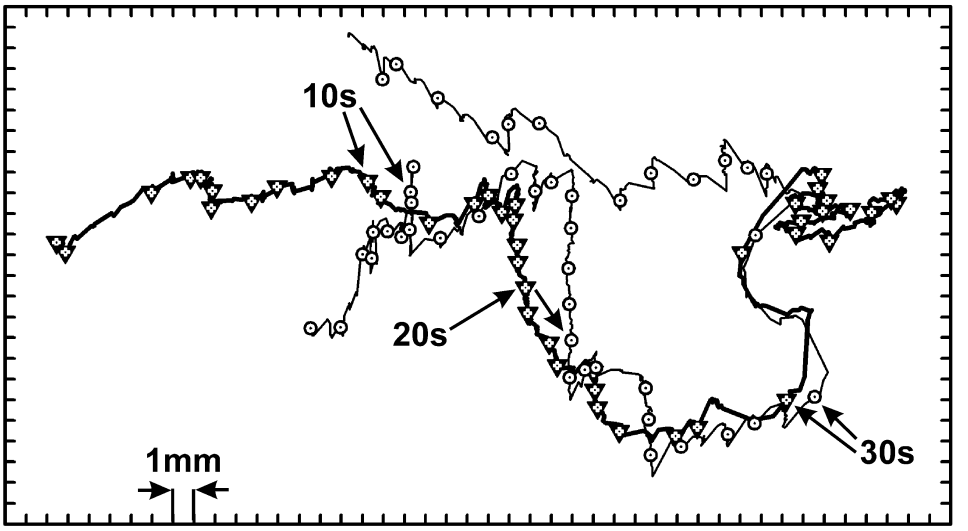

Fig. 3.20. Observation of mating in *Cyclops scutifer*. The male (inverted triangles) swims at random until encountering a female (circles) after 10 s. The male follows the female for the next 20 s; at 30 s they mate. The interval between markers is 1 s.

events were conducted in 1978. However, further detailed observations are required to identify the source of tracking information.

The sensory and behavioral ecology of mating recently has been examined in detail for one important zooplankton group, the copepods [Boxshall (1998); see also the summary by Howlett (1998)]. Several of these papers showed that copepods make use of both chemical and mechanical signals to identify, track, and approach mates, and also to signal their own availability to potential mates (e.g., Yen et al., 1998; Folt and Burns, 1999). In general, chemical trails seem to be the primary basis for long-range (>100 body lengths) detection and tracking (Weissburg et al., 1998), while short-range tracking and recognition uses distinctive hydromechanical cues produced by particular swimming behaviors (Yen et al., 1998) and contact chemoreception (Frey et al., 1998). Search and pursuit swimming behavior is conducted mostly by males. But in at least some cases, females may respond to male chemical exudates with "personal ads" swimming behavior that serves to extend the range and specificity of their detection by males (Howlett, 1998; van Duren et al., 1998).

Detection and pursuit strategies appear to be strongly conditioned by small-scale fluid dynamics. Reliance on chemoreception for long-range detection and tracking is almost certainly because chemical trails last longer (recall that for similar initial gradients, diffusivity of chemical signals is much slower than viscous dissipation of hydromechanical signals) and hence product a longer-lasting interpretable "track." A striking feature in the tracking pattern is that the male does not exactly follow the trajectory of the female (Doall et al., 1998). Instead, the male remains about 1 body length downward from the female trajectory. This orientation is consistent with the chemical signals being "pushed" away from the female body by the downward swimming thrust generated by the female. Yen et al. (1998) noted that the shape and size of successful pursuit trajectories are similar in spatial form to that of the vortex tubes predicted by DNS; they

speculate (as do we) that zooplankton may use transient small-scale fluid structures as channels of sensory and ecological information (Fig. 3.14).

5. Modeling

5.1. From Continuum Ecosystem Models to Lagrangian Approaches

Conventional Continuum Approach

Although mathematical equations for ecosystem dynamics were described earlier, Riley (1946, 1947) first formulated continuum conservation equations for phytoplankton and zooplankton where the interaction and growth terms were expressed in terms of oceanographic factors. He calculated changes in the populations of phytoplankton and zooplankton as a function of time and compared the results with observations. Steele (1974) presented results of simulations with coupled sets of ordinary differential equations for nutrient, phytoplankton biomass, and for each cohort of copepods, individual weight and number of individuals. Nutrients were supplied to the (slab) model by exchange of a set fraction of the slab layer with the reservoir below each day (V in m day^{-1}). Walsh (1975) developed a simulation model of a two-dimensional upwelling ecosystem, where changes were simulated as the ecosystem was advected offshore during active upwelling. A model of plankton patchiness with simultaneous variation in space and time was developed by Wroblewski and O'Brien (1976).

The first widely accepted planktonic ecosystem model was the seven-compartment model of Fasham et al. (1990), which included several recycling pathways but was still simple enough to be evaluated against observations. Again, populations, not individuals, were modeled. Vertical physical processes were represented by an exchange coefficient as in Steele (1974) and a prescribed annual cycle in mixed layer thickness. This continuum model and similar models have been embedded in circulation models (e.g., Fasham et al., 1993; Sarmiento et al., 1993; McGillicuddy et al., 1995b) and in one-dimensional turbulent closure mixed layer models (e.g., Doney, 1966; Doney et al., 1996; Prunet et al., 1996; Denman and Peña, 1999; Wiggert et al., 2000). There seems to be reasonable agreement between observed data and models for nutrient and phytoplankton distributions. However, modeled zooplankton distributions often differ significantly from observations (Olson et al., 1994). Therefore, improved models must incorporate some behavioral aspects of zooplankton, as well as the motility of certain phytoplankton species.

How to Deal with Discreteness of Zooplankton and Phytoplankton

Generally, horizontal circulation models do not yet have the resolution to advect individual organisms on the scales at which they are affected behaviorally (millimeters to tens of meters). However, a number of studies have been seeded with individuals [in individual-based models or (IBMs)] to see how their patterns might be affected by advection, usually in the vicinity of irregular coastal topography. In reality, these individuals are just tags for groups of organisms that would be advected by the flow patterns. Usually, such models are applied to zooplankton (e.g., Werner et al., 1993; Lynch et al., 1998; Miller et al., 1998; Hermann et al., 2001) and to larval fish, with the objective of determining where zooplankton might occur in high concentrations as a food source for fish, or whether larval fish might be dispersed or be contained in some region. These studies are dealt with in greater detail in other chapters.

In ecosystem models, phytoplankton may be divided into two or more species or size classes (e.g., Evans, 1988) with different functional dependencies (on light, nutrients, or grazing) or differential sinking rates (e.g., Boyd and Newton, 1999) such that the individual species or size classes will evolve in time independently (e.g., Fasham et al., 1999). The interaction of individual phytoplankters with a variable flow field associated with a semidiurnal internal tide was first modeled by Kamykowski (1979), and the evolution of the distributions of individual phytoplankton seeded in a prescribed Langmuir cell was first modeled by Evans and Taylor (1980). In both cases, the flow field must be resolved on the same spatial scales as the organisms can move (either through advection or swimming) in a time step. Woods and Onken (1982) developed a Lagrangian model applied to a one-dimensional mixed layer model. Subsequently, Yamazaki and Kamykowski (1991) used an Ekman layer dynamics model coupled with an IBM to study evolving distributions of motile phytoplankton.

Age or Stage, Weight and Number Models for Zooplankton

There is a long history of structured population models of phytoplankton, where in addition to equations for the number of individuals and the weight per individual, there are also equations describing the development of the organisms, through some combination of specifying their age and their developmental stage (see Carlotti et al., 2000; see also other chapters in this volume]. For copepods, Wroblewski (1980) constructed four-stage model with temperature-dependent development rates that was embedded in a two-dimensional time-varying upwelling circulation model. The copepod model was an Eulerian or continuum model with transition rates in and out of each stage compartment at each gridpoint. Davis (1984) developed a similar continuum model with 13 stages, embedded in a model of mean circulation around Georges Bank. Hofmann and Ambler (1988) developed a continuum model with five copepod stages and two size classes of phytoplankton which was then embedded in an objectively derived time-varying flow field of the outercontinental shelf off the southeastern United States which is affected by Gulf Stream meanders.

Another approach to age/stage modeling is to introduce cohorts (or many individuals) into a model at different times and follow the progression of those cohorts/individuals with time (Steele, 1974; Landry, 1976). Similar models with much more complex flow fields have progressively yielded more realistic pictures of the biological–physical flow interactions. In particular, individual-based population models embedded in fine-scale circulation models, where many organisms are tracked as Lagrangian markers of the flow can provide testable predicted distributions of organisms as a function of time and space (e.g., Lynch et al., 1998; Miller et al., 1998; and Hermann et al., 2001).

How to Model Rates That Adapt to Changes in the Environment

In the first approximation, the adapting or variable property, such as the cellular chlorophyll/carbon ratio of phytoplankton, can be instantaneously dependent on the simultaneous environment cue. For example, upward swimming speed of a dinoflagellate could be a function of instantaneous light level. However, the adapting property is often a function of the recent history of the environmental cue. In phytoplankton, photosynthetic parameters vary with ambient light level, but not instantaneously. In the case of the cellular chlorophyll/carbon ratio, the adaptation time may be hours to days because the cell must synthesize (or destroy and eliminate) chlorophyll.

Although the functional relationships that describe biological rates in terms of other variables may be nonlinear, generally the parameters that specify the (nonlinear) functional relationships can be considered to respond to changes in the environment according to linear system response theory. Falkowski and Wirick (1981) considered that the chlorophyll/carbon ratio of individual cells R adapts toward a target value R_w that would be fully adapted to high light according to the first-order adaptation equation

$$\frac{dR}{dt} = \gamma(R_w - R) \tag{23}$$

where γ is an adaptation rate constant. Denman and Marra (1986) were able to determine an adaptation time scale $(\gamma)^{-1}$ from culture observations at different light levels, where the parameter undergoing adaptation to ambient light was P_m, the asymptotic maximum value in the phytoplankton production versus light relationship. They were then able to use the time-varying (due to adaptation of P_m) production versus light relationship to simulate observations of instantaneous photosynthetic oxygen production and incident radiation. Franks and Marra (1994) and Farmer and McNeil (1999) extended this type of analysis into a bulk mixed laye model environment.

5.2. Lagrangian Models

Lagrangian Motion of Organisms as a Random Walk Process

As an alternative to direct numerical simulation of the Lagrangian transport of organisms in small-scale turbulence, it is appealing to represent the Lagrangian motion as a random walk process. Yamazaki and Kamykowski (1991) and Kamykowski et al. (1994) have explored the interaction of directed vertical swimming and of the photo-adaptation of the photosynthetic response by a random walk representation of turbulent motions in the upper ocean, with a vertical diffusive coefficient that varied vertically and with time. The results were able to demonstrate individual interactions with the simulated vertical turbulence. However, Holloway (1994) pointed out that applying the same vertically variable random walk in some idealized situations can lead to physically unrealistic "unmixing." Yamazaki and Kamykowski (1994) noted that the difference between stochastic calculus and random walks is not trivial to resolve. The conventional random walk technique, which is equivalent to the Ito calculus, leads to the Fokker–Planck equation, whereas the Stratonovich calculus reduces to the Fickian diffusin equation.

Okubo (1986) demonstrated the relationship between stochastic calculus and a generalized random walk. He considered a one-dimensional discrete random walk: for a particle at a time step m and a location i, chose the next step either toward the right or the left with a fixed step, or no motion. The sum of the transition probability toward the right, k^+ $(i, i + 1; m)$, the probability remaining at the same location, $k_0(i; m)$, and the transition probability toward the left, k^- $(i, i - 1; m)$, follow the conservation law;

$$k^+(i, i + 1; m) + k^-(i, i - 1; m) + k_0(i; m) = 1 \tag{24}$$

The density of particles at location i and time step m, $p(i, m)$, is expressed in terms of the particle density at the previous time step at three different locations:

$$p(i, m+1) = k^{+}(i-1, i; m)p(i-1, m) + k^{-}(i+1, i; m)p(i+1, m) + k_0(i; m)p(i, m) \quad (25)$$

In a general derivation, the transition probability can be evaluated anywhere between the departing point and the arrival point during the time step m to $m + 1$. The Ito calculus corresponds to a departing point evaluation, and the Stratonovich calculus corresponds to a middle point evaluation. Depending on how the probability is evaluated, two different equivalent continuous equations are derived. When there is no bias in the transitional probability, which is equivalent to no advective effect, the Ito calculus leads to the Fokker–Planck equation:

$$\frac{\partial p}{\partial t} = -\frac{\partial^2}{\partial x^2}\,(Kp) \quad (26)$$

and the Stratonovich calculus leads to the Fickian diffusion equation:

$$\frac{\partial p}{\partial t} = -\frac{\partial}{\partial x}\left(K\,\frac{\partial p}{\partial x}\right) \quad (27)$$

where K is the diffusion coefficient. Usually, the traditional random walk is based on the Ito calculus, when a particle is advanced in time and the transition probability is evaluated at the departing point. To be more specific, the location of each particle at time step $m + 1$ is expressed as a function of the previous time step and a Gaussian random variable:

$$X(m+1) = X(m) + N(0, 2K(X(m))) \quad (28)$$

where $N(0, 2K(X(m)))$ is a Gaussian random variable with zero mean and variance $2K(X(m))$. The Stratonovich calculus is equivalent to the following random walk:

$$X(m+1) = X(m) + N\left(0, 2K\left(\frac{X(m+1) + X(m)}{2}\right)\right) \quad (29)$$

If equation 29 is consistent with the Fickian diffusion equation, an unmixing situation will not occur. The diffusivity value is determined from the midpoint between the departure and the arrival point. However, this is not an easy task to implement in a general numerical simulation, because the operation requires an iterative method. So it is not surprising to obtain a result inconsistent with physical reality. As Holloway (1994) noted, the traditional random walk collects particles in low-diffusivity regions. This tendency is merely the result of mathematics, not physics.

To resolve the inconsistency, Hunter et al. (1993) developed a compensating technique to remove the physically unrealistic unmixing tendency:

$$X(m+1) = X(m) + N(0, 2K(X(m))) + \frac{\partial K(X(m))}{\partial x} \tag{30}$$

Visser (1997) proposed a more theoretically rigorous correction method:

$$X(m+1) = X(m) + N\left(0, 2K\left(X(m) + \frac{1}{2}\,\frac{\partial K(X(m))}{\partial x}\right)\right) + \frac{\partial K(X(m))}{\partial x} \tag{31}$$

His simulations demonstrated the unrealistic unmixing. Yamazaki and Li (unpublished manuscript) have performed a similar simulation to test whether the Stratonovich calculus is consistent with the Fickian diffusion equation. Interestingly, the Stratonovich random walk (equation 29) requires half the correction proposed by Hunter et al. (1993) and Visser (1997). Yamazaki and Li have also found that either correction, equation 30 or 31, yields the same steady-state results for a modulatory changing K. The lesson from these recent random walk simulations is that by adding the simple correction term of Visser (1997), the physically unrealistic bias due to variable diffusivity is avoided. According to the derivation of Okubo (1986), the Stratonovich calculus and Fickian diffusion are consistent with each other; however, the Stratonovich random walk will unmix a uniform distribution of particles unless the correction is applied. This apparent contradiction is still an unresolved mystery. The answer may rest with the difficulty in expressing the stochastic differentials, such that the conventional Taylor expansion used to link the discrete and the continuous case is not applicable.

A related problem, how to advect individual organisms, arises when individual-based models (IBMs) for motile plankton are coupled with a compartment-based lower foodweb model in a mixed layer model. The Mellor–Yamada family of mixed layer models produce time-varying TKE, $\frac{1}{2}\overline{q^2}$ and $\overline{q^2 l}$ where l is the turbulence length scale. The turbulence time scale can be calculated (D'Alessio et al., 1998) as $\tau_t = c_3 l/q$, with $c_3 = 1.56$. In addition, the eddy diffusion coefficient for passive scalars is, by definition, $K_h = \tau_t \overline{w'^2}$. We thus have the rms vertical velocity and the turbulent time scale from which we can simulate the movement of individual organisms by turbulent transport via random walk simulations. Each particle is moved by an amount obtained from the Gaussian distribution with mean zero and the standard deviation $(2K_h\tau_t)^{1/2}$ for a τ_t time duration. We need to take into consideration the correction method for the variable diffusivity problem, but its straightforward application to mixed layer models requires careful attention. All the variable diffusion simulations are made for a continuous analytical diffusion coefficient, where the derivative of diffusivity exists everywhere in the computational domain. On the other hand, mixed layer models provide a diffusivity value only at discrete grid points, requiring an interpolation to obtain a derivative at the grid point. A clear procedure to estimate well-behaved derivatives at the grid points is not yet available.

A second problem with representing vertical motion in the mixed layer as a random walk process was pointed out by Yamazaki and Kamykowski (1991): The simulations do not produce large excursions of organisms over the entire mixed layer, contrary to observations with neutrally buoyant floats (e.g., D'Asaro et al., 1996). The lack of parameterization of large energy-containing eddies is a more general problem in TKE mixed layer models, which Large et al. (1994) and D'Alessio et al. (1998) have

tried to address by scaling the vertical diffusion according to a diagnosed mixed layer thickness, incorporating the nonlocal representations developed from LES modeling.

Including Behavior Aspects into Planktonic Ecosystem Models

The next step in examining adaptation is the adjustment of buoyancy or active swimming in response to environmental cues. Now the adapted behavior results not just in a variable sink or source, but in directed motion that must be treated as a variable advection or diffusion term. Okubo (1980) examined the general problem of interacting populations in a diffusive medium. Davis et al. (1991) developed a series of simple models where zooplankton alter their motion in the presence of higher prey concentrations. They also examined the effects of different levels of turbulence on patchy feeding interactions. Kamykowski et al. (1994) modeled observations of swimming dinoflagellates undervariable environmental conditions.

There are two important biological behavioral traits to model: (1) grouping (aggregation) and (2) foraging. Unfortunately, only limited effort has been spent on Lagrangian modeling. Yamazaki (1993) briefly reviewed the related work in this area and introduced two modeling approaches for aggregation. One is a modification of the Langevin equation (Yamazaki and Okubo, 1995). The other (Yamazaki and Haury, 1993) augments a pure random walk (turbulent diffusion) with an "attractive" force toward higher concentrations of particles, which is modeled by a nonparametric probability density function technique. This type of modeling work must eventually be integrated into the numerical simulation of turbulence. An important aspect of the Lagrangian models is that the formulation should not mix a physically driven step with a biologically originating step. For instance, a one-dimensional formulation of a Lagrangian model ought to be expressed as

$$X(m+1) = X(m) + W_P(m) + W_B(m) \tag{32}$$

where W_P is the physical step and W_B is the biological step.

No realistic foraging behavior model has yet appeared in the literature. Traditional modeling studies examine the sensitivity of the parameterizations of a biological system, but the parameters normally remain fixed during the entire simulation. However, fixed parameterization is not realistic for behavior models of organisms, because each organism is presumably responding to its constantly changing environment. A new modeling strategy must incorporate this sort of biological decision. Laboratory observations of individual plankters should be integrated into such a modeling effort with existing knowledge of sensory mechanisms. Following this approach, Keiyu et al. (1994) attempted to mimic the swimming behavior of copepods by making use of an adaptive behavior approach. Yamazaki and Kamykowski (2000) extend the adaptive behavior model to simulate the one-dimensional swimming behavior of a dinoflagellate by taking account of the internal physiological conditions. An elaborated behavior model for zooplankton calls for more attention.

Acknowledgments

Support for this work was provided by Grant-in-Aid for Scientific Research (C) 10045026 (to H.Y.) and by Fisheries and Oceans Canada and the Canadian GLOBEC and JGOFS programs (to D.L.M. and K.L.D.). The sections on zooplankton sensory

ecology and feeding behavior benefited greatly from discussions with Marie Bundy, Petra Lenz, Mimi Koehl, Rudi Strickler and Jeanette Yen. We thank the editors and anonymous reviewers for helpful comments.

References

Agrawal, Y. C., E. A. Terray, M. A. Donelan, M. A. Hwang, A. J. Williams III, W. M. Drennan, K. K. Kahma and K. K. Kitaigorodskii, 1992. Enhanced dissipation of kinetic energy beneath surface waves. *Nature*, **359,** 219–233.

Alcaraz, M., 1997. Turbulence and copepods: grazing, behavior and metabolic rates. *Sci. Mar.*, **61**(Suppl. 1), 177–195.

Anis, A. and J. N. Moum, 1992. The superadiabatic surface layer of the ocean during convection. *J. Phys. Oceanogr.*, **22,** 1221–1227.

Anselmet, F., Y. Gagne, E. J. Hopfinger and R. A. Atonia, 1984. High-order velocity structure functions in turbulent shear flows. *J. Fluid Mech.*, **140,** 63–89.

Atema, J., R. R. Fay, A. N. Popper and W. N. Tavolga, eds., 1988. *Sensory Biology of Aquatic Animals*. Springer-Verlag, New York.

Bollens, S. M., B. W. Frost and J. R. Cordell, 1994. Chemical, mechanical and visual cues in the vertical migration behavior of the marine planktonic copepod *Acartia hudsonica. J. Plankton Res.*, **16,** 555–564.

Boxshall, G. A., ed., 1998. Mating biology of copepod crustaceans. *Philos. Trans. R. Soc. London Ser. B*, **353,** 669–815.

Boyd, P. W. and P. P. Newton, 1999. Does planktonic community structure determine downward particulate organic carbon flux in different oceanic provinces? *Deep-Sea Res. I*, **46,** 63–91.

Bleckman, H., T. Breihaupt, R. Blickhan and J. Tautz, 1991. The time course and frequency content of hydrodynamic events caused by moving fish, frogs, and crustaceans. *J. Comp. Physiol. A*, **168,** 749–757.

Budelmann, B.-U., 1988. Morphological diversity of equilibrium receptor systems in aquatic invertebrates. In *Sensory Biology of Aquatic Animals*, J. Atema, R. R. Fay, A. N. Popper and W. N. Tavolga, eds. Springer-Verlag, New York, pp. 757–782.

Bundy, M. H. and G.-A. Paffenhoffer, 1996. Analysis of flow fields associated with freely swimming calanoid copepods. *Mar. Ecol. Prog. Ser.*, **133,** 99–113.

Bundy, M. H., T. F. Gross, H. A. Vanderploeg and J. R. Strickler, 1998. Perception of inert particles by calanoid copepods: behavioral observations and a numerical model. *J. Plankton Res.*, **20,** 2129–2152.

Buskey, E. J., J. O. Peterson and J. W. Ambler, 1996. The swarming behavior of the copepod *Dioithona oculata*: in situ and laboratory studies. *Limnol. Oceanogr.*, **41,** 513–521.

Carlotti, F., J. Giske and F. Werner, 2000. Modelling zooplankton dynamics. In *ICES Zooplankton Methodology Manual*, R. Harris, P. Wiebe, J. Lenz, H-R Skjoldal and M. Huntley, eds. Academic Press, pp. 571–667.

Cassie, R. M., 1963. Microdistribution of plankton. *Oceanogr. Mar. Biol. Annu. Rev.*, **1,** 223–252.

Clark, C. W. and D. A. Levy, 1988. Diel vertical migrations by juvenile sockeye salmon and the antipredation window. *Am. Nat.* **131,** 271–290.

Costello, J. H. and S. P. Colin, 1994. Morphology, fluid motion and predation by the seyphomedusa *Aurelia aurita. Mar. Biol.*, **121,** 327–334.

Costello, J. H., J. R. Strickler, C. Marrasé, G. Trager, R. Zeller and A. T. Friese, 1990. Grazing in a turbulent environment: behavioral responses of a calanoid copepod, *Centropages hamatus. Proc. Natl. Acad. Sci. USA*, **87,** 1648–1652.

Cowles, T. and P. Donaghay, 1998. Thin layers: observations of small-scale patterns and processes in the upper ocean. *Oceanography*, **11,** 2.

Cowles, T. J., R. J. Olson and S. W. Chisholm, 1988. Food selection by copepods: discrimination on the basis of food quality. *Mar. Biol.*, **100,** 41–49.

Cowles, T. J., R. A. Desiderio and M. E. Carr, 1998. Small-scale planktonic structure: persistence and trophic consequences. *Oceanography*, **11,** 4–9.

Craik, A. D. and S. Leibovich, 1976. A rational model for Langmuir circulation. *J. Fluid Mech.*, **73,** 401–426.

D'Alessio, S. J. D., K. Abdella and N. A. McFarlane, 1998. A new second-order turbulence closure scheme for modeling the oceanic mixed layer. *J. Phys. Oceanogr.*, **28,** 1624–1641.

D'Asaro, E. A., 1989. The decay of wind-forced mixed layer inertial oscillations due to the β effect. *J. Geophys. Res.*, **94,** 2045–2056.

D'Asaro, E. A., D. M. Farmer, J. T. Osse and G. T. Dairiki, 1996. A Lagrangian float. *J. Atmos. Ocean. Technol.*, **13,** 1230–1246.

Davis, C. S., 1984. Interaction of a copepod population with the mean circulation on Georges Bank. *J. Mar. Res.*, **42,** 573–590.

Davis, C. S., G. R. Flierl, P. H. Wiebe and P. J. Franks, 1991. Micropatchiness, turbulence and recruitment in plankton. *J. Mar. Res.*, **49,** 109–151.

Davis, C. S., S. M. Gallager and A. R. Solow, 1992. Microaggregations of oceanic plankton observed by towed video microscopy. *Science*, **257,** 230–232.

Davis, A. D., T. M. Weatherby, D. K. Hartline and P. H. Lenz, 1999. Myelin-like sheaths in copepod axons. *Nature*, **398,** 571.

DeMott, W. R. and M. D. Watson, 1991. Remote detection of algae by copepods: responses to algal size, odors and motility. *J. Plankton Res.*, **13,** 1203–1222.

Denman, K. L., 1984. Predictability of the marine planktonic ecosystem. In *Predictability of Fluid Motions*, G. Holloway and B. West, eds. American Institute of Physics, New York, pp. 601–602.

Denman, K. L. and J. Marra, 1986. Modelling the time dependent photoadaptation of phytoplankton to fluctuating light. In *Marine Interface Ecohydrodynamics*, J. C. J. Nihoul, ed. Elsevier, Amsterdam, pp. 341–359.

Denman, K. L. and M. Miyake, 1973. Upper layer modification at Ocean Station Papa: observations and simulation. *J. Phys. Oceanogr.*, **3,** 185–196.

Denman, K. L. and M. A. Peña, 1999. A coupled 1-D biological/physical model of the northeast subarctic Pacific ocean with iron limitation. *Deep-Sea Res. II*, **46,** 2877–2908.

Denman, K. L. and T. M. Powell, 1984. Effects of physical processes on planktonic ecosystems in the coastal ocean. *Oceanogr. Mar. Biol. Annu. Rev.*, **22,** 125–168.

Dewey, R. K. and J. N. Moum, 1990. Enhancement of fronts by vertical mixing. *J. Geophys. Res.*, **95,** 9433–9446.

Dillon, T. M., 1982. Vertical overturns: a comparison of Thorpe and Ozmidov length scales. *J. Geophys. Res.*, **87,** 9601–9613.

Doall, M. H., S. P. Colin, J. R. Strickler and J. Yen, 1998. Locating a mate in 3D: the case of *Temora longicornis*. *Philos. Trans. R. Soc. London Ser. B*, **353,** 681–689.

Doney, S. C., 1996. A synoptic atmospheric surface forcing data set and physical upper ocean model for the U.S. JGOFS Bermuda Atlantic Time-Series Study site. *J. Geophys. Res.*, **101,** 25615–25634.

Doney, S. C., D. M. Glover and R. G. Najjar, 1996. A new coupled, one-dimensional biological–physical model for the upper ocean: applications to the JGOFS Bermuda Atlantic Time Series (BATS) site. *Deep-Sea Res. II*, **43,** 591–624.

Dower, J. F., T. J. Miller and W. C. Leggett, 1997. The role of microscale turbulence in the feeding ecology of larval fish. *Adv. Mar. Biol.*, **31,** 170–220.

Dusenbery, D. B., 1992. *Sensory Ecology: How Organisms Acquire and Respond to Information*. W.H. Freeman, New York.

Evans, G. T., 1988. A framework for discussing seasonal succession and coexistence of phytoplankton species. *Limnol. Oceanogr.*, **33,** 1027–1036.

Evans, G. T. and F. J. R. Taylor, 1980. Phytoplankton accumulation in Langmuir cells. *Limnol. Oceanogr.*, **25,** 840–845.

Falkowski, P. G. and C. D. Wirick, 1981. A simulation model of the effects of vertical mixing on primary productivity. *Mar. Biol.*, **65,** 69–75.

Farmer, D. M. and M. Li, 1995. Patterns of bubble clouds organized by Langmuir circulation. *J. Phys. Oceanogr.*, **25,** 1426–1440.

Farmer, D. M. and C. McNeil, 1999. Photoadaptation in a convective layer. *Deep-Sea Res. II*, **46,** 2433–2446.

Fasham, M. J. R., H. W. Ducklow and S. M. McKelvie, 1990. A nitrogen-gased model of plankton dynamics in the oceanic mixed layer. *J. Mar. Res.*, **48,** 591–639.

Fasham, M. J. R., J. L. Sarmiento, R. D. Slater, H. W. Ducklow and R. Williams, 1993. Ecosystem behavior at Bermuda Station "S" and Ocean Weather Station "India": a general circulation model and observational analysis. *Global Biogeochem. Cycles*, **7,** 379–415.

Fasham, M. J. R., P. W. Boyd and G. Savidge, 1999. Modeling the relative contributions of autotrophs and heterotrophs to carbon flow at a Lagrangian JGOFS station in the northeast Atlantic: the importance of DOC. *Limnol. Oceanogr.*, **44,** 80–94.

Fields, D. M. and J. Yen, 1996. The escape behavior of *Pleuromamma xiphias* in response to a quantifiable fluid mechanical disturbance. In *Zooplankton: Sensory Ecology and Physiology*, P. H. Lenz, D. K. Hartline, J. E. Purcell and D. L. Macmillan, eds. Gordon & Breach, Amsterdam, pp. 323–340.

Fields, D. M. and J. Yen, 1997. The escape behavior of marine copepods in response to a quantifiable fluid mechanical disturbance. *J. Plankton Res.*, **19,** 1289–1304.

Folt, C. L. and C. W. Burns, 1999. Biological drivers of zooplankton patchiness. *Trends Ecol. Evol.*, **14,** 300–305.

Franks, P. J. and J. Marra, 1994. A simple new formulation for phytoplankton photoresponse and an application in a wind-driven mixed-layer model. *Mar. Ecol. Prog. Ser.*, **111,** 143–153.

Frey, M. A., D. J. Lonsdale and T. W. Snell, 1998. The influence of contact chemical signals on mate recognition in a harpacticoid copepod. *Philos. Trans. R. Soc. London Ser. B*, **353,** 745–791.

Friedman, M. M., 1980. Comparative morphology and functional significance of copepod receptors and oral structures. In *Evolution and Ecology of Zooplankton Communities*, W. M. Kerfoot, ed. New England University Press, Hanover, N.H., pp. 185–197.

Gallager, S. M., C. S. Davis, A. W. Epstein, A. Solow and R. C. Beardsley, 1996. High-resolution observations of plankton spatial distributions correlated with hydrography in the Great South Channel, Georges Bank. *Deep-Sea Res. II*, **43,** 1627–1663.

Gargett, A., 1989. Ocean turbulence. *Annu. Rev. Fluid Mech.*, **21,** 419–451.

Gargett, A., 1997. "Theories" and techniques for observing turbulence in the ocean euphotic zone. *Sci. Mar.*, **61**(Suppl. 1), 25–45.

Gargett, A., T. R. Osborn and P. W. Nasmyth, 1984. Local isotropy and the decay of turbulence in a stratified fluid. *J. Fluid Mech.*, **144,** 231–280.

Gaspar, P., 1988. Modeling the seasonal cycle of the upper ocean, *J. Phys. Oceanogr.*, **18,** 161–180.

Gaspar, P., Y. Gregoris and J. M. Lefevre, 1990. A simple eddy kinetic energy model for simulations of the oceanic vertical mixing: test at station Papa and the long term upper ocean study site. *J. Geophys. Res.*, **95**, 16179–16193.

Genin, A., Lazar and Brenner. 1995. Vertical mixing and coral death in the Red Sea following the eruption of Mount Pinatubo. *Nature*, **377,** 507–510.

Gerristsen, J. and J. R. Strickler, 1977. Encounter probabilities and community structure in zooplankton: a mathematical model. *J. Fish. Res. Board Can.*, **34,** 73–82.

Gill, C. W., 1986. Suspected mechao- and chemosensory structures of *Temora Iongicornis* (Copepoda: Calanoida). *Mar. Biol.*, **93,** 449–457.

Gill, C. W. and D. J. Crisp, 1985. Sensitivity of intact and antennule-amputated copeods to water disturbance. *Mar. Ecol. Prog. Ser.*, **21,** 221–227.

Granata, T. C. and T. D. Dickey, 1991. The fluid mechanics of copepod feeding in a turbulent flow: a theoretical approach. *Prog. Oceanogr.*, **26,** 243–261.

Grant, H. L., R. W. Stewart and A. Moilliet, 1962. Turbulence spectra form a tidal channel. *J. Fluid Mech.*, **12,** 241–268.

Gregg, M. C. 1987. Diapycnal mixing in the thermocline: a review. *J. Geophys. Res.*, **92,** 5249–5286.

Gurvich, A. S. and A. M. Yaglom, 1967. Breakdown of eddies and probability distributions for small scale turbulence. *Phys. Fluids A*, **1,** 186–189.

Hamner, W. M., 1985. The importance of ethology for investigations of marine zooplankton. *Bull. Mar. Sci.*, **37,** 414–424.

Hamner, P. and W. M. Hamner, 1977. Chemosensory tracking of scent trails by the planktonic shrimp *Acetes sibogae australis. Science*, **195,** 886–888.

Hanson, A. K., Jr. and P. L. Donaghay, 1998. Micro- to fine-scale chemical gradients and layers in stratified coastal waters. *Oceanography*, **11,** 10–17.

Hartline, D. K., P. H. Lenz and C. M. Herren, 1996. Physiological and behavioral studies of escape responses in calanoid copepods. *Mar. Freshw. Behav. Physiol.*, **27,** 199–212.

Haury, L. R. and H. Yamazaki, 1995. The dichotomy of scales in the perception and aggregation behavior of zooplankton. *J. Plankton Res.*, **17,** 191–197.

Haury, L. R., H. Yamazaki and E. C. Itsweire, 1990. Effects of turbulent shear flow on zooplankton distribution. *Deep-Sea Res.*, **37,** 447–461.

Hermann, A. J., S. Hinckley, B. A. Megrey and J. M. Napp, 2001. Applied and theoretical considerations for constructing spatially explicit individual-based models of marine fish early life history which include multiple trophic levels. *ICES J. Mar. Sci.* (in press).

Hofmann, E. E. and J. W. Ambler, 1988. Plankton dynamics on the outer southeastern U.S. continental shelf. II. A time-dependent biological model. *J. Mar. Res.*, **46,** 883–917.

Holliday, D. V., R. E. Pieper, C. F. Greenlaw and J. K. Dawson, 1998. Acoustical sensing of small-scale vertical structures in zooplankton assemblages. *Oceanography*, **11,** 18–23.

Holloway, G., 1994. On modeling vertical trajectories of phytoplankton in a mixed layer. *Deep-Sea Res. I*, **41,** 957–959.

Howlett, R., 1998. Sex and the single copepod. *Nature*, **394,** 423–424.

Hunter, J. R., P. D. Craig and H. E. Phillips, 1993. On the use of random walk models with spatial variable diffusivity. *J. Comput. Phys.*, **106,** 366–376.

Incze, L. S., P. Aas and T. Ainaire, 1996. Distributions of copepod nauplii and turbulence on the southern flank of Georges Bank: implications for feeding by larval cod (*Gadus morhua*). *Deep-Sea Res. II*, **43,** 1855–1873.

Jaffe, J. S., P. J. S. Franks and A. W. Leising, 1998. Simultaneous imaging of phytoplankton and zooplankton distributions. *Oceanography*, **11,** 24–29.

Jiménez, J., 1992. Kinematic alignment effects in turbulent flows. *Phys. Fluids A*, **4,** 652–654.

Jiménez, J., 1997. Oceanic turbulence at millimeter scales. *Sci. Mar.*, **61**(Suppl. 1), 47–56.

Jou, D., 1997. Intermittent turbulence: a short introduction. *Sci. Mar.*, **61**(Suppl. 1), 57–62.

Kamykowski, D., 1979. The growth response of a model *Gymnodinium splendens* in stationary and wavy water columns. *Mar. Biol.*, **50,** 289–303.

Kamykowski, D., H. Yamazaki and G. S. Janowitz, 1994. A Lagrangian model of phytoplankton photosynthetic response in the upper mixed layer. *J. Plankton Res.*, **16,** 1059–1069.

Kantha, L. H. and C. A. Clayson, 1994. An improved mixed layer model for geophysical applications. *J. Geophys. Res.*, **99,** 25235–25266.

Keiyu, A. Y., H. Yamazaki and J. R. Strickler, 1994. A new modelling approach for zooplankton behaviour. *Deep-Sea Res. II*, **41,** 171–184.

Kerfoot, W. M., ed., 1980. *Evolution and Ecology of Zooplankton Communities*. New England University Press, Hanover, N.H.

Kerr, R. M., 1985. Higher-order derivative correlations and the alignment of small-scale structures in isotropic numerical turbulence. *J. Fluid Mech.*, **153,** 31–58.

Kiorboe, T., 1997. Small-scale turbulence, marine snow formation, and planktivorous feeding. *Sci. Mar.*, **61**(Suppl. 1), 141–158.

Kiorboe, T. and B. MacKenzie, 1995. Turbulence-enhanced prey encounter rates in larval fish: effects of spatial scale, larval behaviour and size. *J. Plankton Res.*, **17,** 2319–2331.

Kiorboe, T. and E. Saiz, 1995. Planktivorous feeding in calm and turbulent environments, with emphasis on copepods. *Mar. Ecol. Prog. Ser.*, **122,** 135–145.

Kiorboe, T. and A. W. Visser, 1999. Predator and prey perception in copepods due to hydromechanical signals. *Mar. Ecol. Prog. Ser.*, **179,** 81–95.

Kiorboe, T., E. Saiz and A. W. Visser, 1999. Hydrodynamic signal perception in the copepod *Acartia tonsa. Mar. Ecol. Prog. Ser.*, **179,** 97–111.

Kitaigorodskii, S. A., M. A. Donelan, J. L. Lumley and E. A. Terray, 1983. Wave–turbulence interaction in the upper ocean. 2. Statistical characteristics of wave and turbulent components of the random velocity field in the marine surface layer. *J. Phys. Oceanogr.*, **13,** 1988–1999.

Koehl, M. A. and J. R. Strickler, 1981. Copepod feeding currents: food capture at low Reynolds number. *Limnol. Oceanogr.*, **26,** 1062–1073.

Kolmogorov, A. N., 1941a. Local turbulent structure in incompressible fluids at very high Reynolds number. *Dokl. Akad. Nauk SSSR*, **30,** 299–303.

Kolmogorov, A. N., 1941b. On the logarithmical normal particle size distribution caused by particle crushing. *Dokl. Akad. Nauk SSSR*, **31,** 99–102.

Kolmogorov, A. N., 1962. A refinement of previous hypotheses concerning the local structure of turbulence in a viscous incompressible fluid at high Reynolds number. *J. Fluid Mech.*, **13,** 82–85.

Kraus, E. B. and J. S. Turner, 1967. A one-dimensional model of the seasonal thermocline. II. The general theory and its consequences. *Tellus*, **19,** 98–106.

Krebs, J. R. and N. B. Davies, 1981. *An Introduction to Behavioral Ecology.* Sinauer Associates, Sunderland, Mass.

Kundu, P., 1990. *Fluid Mechanics.* Academic Press, San Diego, Calif.

Landry, M. R., 1976. The structure of marine ecosystems: an alternative. *Mar. Biol.*, **35,** 1–7.

Langmuir, I., 1938. Surface motion of water induced by wind. *Science*, **87,** 119–123.

Large, W. G., J. C. McWilliams and S. C. Doney, 1994. Ocean vertical mixing: a review and a model with a nonlocal boundary layer parameterization. *Rev. Geophys.*, **32,** 363–403.

Leibovich, S. and A. Tandon, 1993. Three dimensional Langmuir circulation instability in a stratified layer. *J. Geophys. Res.*, **98,** 16501–16507.

Lenz, P. H., D. K. Hartline, J. E. Purcell and D. L. Macmillan, eds., 1996a. *Zooplankton: Sensory Ecology and Physiology.* Gordon & Breach, Amsterdam.

Lenz, P. H., T. M. Weatherby, W. Weber and K. K. Wong, 1996b. Sensory specialization along the first antenna of a calanoid copepod, *Pleuromamma xiphias* (Crustacea). In *Zooplankton: Sensory Ecology and Physiology*, P. H. Lenz, D. K. Hartline, J. E. Purcell and D. L. Macmillan, eds. Gordon & Breach, Amsterdam, pp. 355–364.

Levich, E., 1987. Certain problems in the theory of developed hydrodynamical turbulence. *Phys. Rep.*, **151,** 129–238.

Levins, R., 1962. Theory of fitness in a heterogeneous environment. I. The fitness set and adaptive function. *Am. Nat.*, **96,** 361–378.

Levins, R., 1968. *Evolution in Changing Environments: Some Theoretical Explorations*. Princeton University Press, Princeton, N.J.

Levins, R. and R. MacArthur, 1966. Maintenance of genetic polymorphism in a heterogeneous environment: variations on a theme by Howard Levene. *Am. Nat.*, **100,** 585–590.

Li, M. and C. Garrett, 1993. Cell merging and the jet/downwelling ratio in Langmuir circulation. *J. Mar. Res.*, **51,** 737–769.

Li, M. and C. Garrett, 1995. Is Langmuir circulation driven by surface waves or surface cooling? *J. Phys. Oceanogr.*, **25,** 64–76.

Li, M. and C. Garrett, 1997. Mixed layer deepening due to Langmuir circulation. *J. Phys. Oceanogr.*, **27,** 121–132.

Li, M., Zahariev, K. and C. Garrett, 1995. Role of Langmuir circulation in the deepening of the ocean surface mixed layer. *Science*, **270,** 1955–1957.

Lueck, R. G., 1988. Turbulent mixing at the Pacific subtropical front. *J. Phys. Oceanogr.*, **18,** 1761–1774.

Lynch, D. R., W. C. Gentleman, D. J. McGillicuddy, Jr. and C. S. Davis, 1998. Biological/physical simulations of *Calanus finmarchicus* population dynamics in the Gulf of Maine. *Mar. Ecol. Prog. Ser.*, **169,** 189–210.

MacArthur, R. and E. Pianka, 1966. On the optimal use of a patchy environment. *Am. Nat.*, **100,** 603–609.

Mackas, D., H. Sefton, C. Miller and A. Raich, 1993. Vertical habitat partititioning by large calanoid copepods in the oceanic subarctic Pacific during spring. *Prog. Oceanogr.*, **32,** 259–294.

Mackas, D. L., K. L. Denman and M. R. Abbott, 1985. Plankton patchiness: biology in the physical vernacular. *Bull. Mar. Sci.*, **37,** 652–674.

MacKenzie, B. R. and T. Kiorboe, 1995. Encounter rates and swimming behavior of pause-travel and cruise larval fish predators in calm and turbulent laboratory environments. *Limnol. Oceanogr.*, **40,** 1278–1289.

MacKenzie, B. R., T. J. Miller, S. Cyr and W. C. Leggett, 1994. Evidence for a dome-shaped relationship between turbulence and larval fish ingestion rates. *Limnol. Oceanogr.*, **39,** 1790–1799.

Mangel, M. and C. W. Clark, 1986. Towards a unified foraging theory. *Ecology*, **67,** 1127–1138.

Marrasé, C., J. H. Costello, T. Granata and J. R. Strickler, 1990. Grazing in a turbulent environment: energy, dissipation, encounter rates and efficacy of feeding currents in *Centropages hamatus. Proc. Natl. Acad. Sci. USA*, **87,** 1653–1657.

Marrasé, C., E. Saiz and J. M. Redondo, eds. 1997. Lectures on plankton and turbulence. *Sci. Mar.*, **61**(Suppl. 1).

Maynard Smith, J., 1992. *Did Darwin Get It Right? Essays on Games, Sex and Evolution*. Chapman & Hall, London.

McGillicuddy, D. J., Jr., J. J. McCarthy and A. R. Robinson, 1995a. Coupled physical and biological modeling of the spring bloom in the North Atlantic. I. Model formulation and one dimensional bloom processes. *Deep-Sea Res. I*, **42,** 1313–1357.

McGillicuddy, D. J., Jr., J. J. McCarthy and A. R. Robinson, 1995b. Coupled physical and biological modeling of the spring bloom in the North Atlantic. II. Three dimensional bloom and post-bloom processes. *Deep-Sea Res. I*, **42,** 1359–1398.

McWilliams, J. C., P. P. Sullivan and C.-H. Moeng, 1997. Langmuir turbulence in the ocean. *J. Fluid Mech.*, **334,** 1–30.

Mellor, G. L. and P. A. Durbin, 1975. The structure and dynamics of the ocean surface mixed layer. *J. Phys. Oceanogr.*, **5,** 718–728.

Mellor, G. L. and T. Yamada, 1974. A hierarchy of turbulence closure models for planetary boundary layers. *J. Atmos. Sci.*, **31,** 1791–1806.

Mellor, G. L. and T. Yamada, 1982. Development of a turbulent closure model for geophysical fluid problems. *Rev. Geophys. Space Phys.*, **20,** 851–875.

Miller, C. B., D. R. Lynch, F. Carlotti, W. Gentleman and C. W. Lewis, 1998. Coupling of an individual-based population dynamic model of *Calanus finmarchicus* to a circulation model for the Georges Bank region. *Fish. Oceanogr.*, **7,** 219–234.

Mood, A. M., F. A. Graybill and D. C. Boes, 1974. *Introduction to the Theory of Statistics*. McGraw-Hill, New York.

Moum, J. N., D. R. Caldwell and C. A. Paulson, 1989. Mixing in the equatorial surface layer and thermocline. *J. Geophys. Res.*, **94,** 2005–2022.

Oakey, N. S. and J. A. Elliott, 1982. Dissipation within the surface mixed layer. *J. Phys. Oceanogr.*, **12,** 171–185.

Okubo, A., 1980. *Diffusion and Ecological Problems: Mathematical Models.* Biomathematics Series, Vol. 10. Springer-Verlag, New York.

Okubo, A., 1986. Dynamical aspects of animal grouping: swarms, schools, flocks, herbs. *Adv. Biophys.*, **22,** 1–94.

Okubo, A., 1987. The fantastic voyage into the deep: marine biofluid mechanics. In *Mathematical Topics in Population Biology, Morphogenesis, and Neurosciences*, E. Teramoto and M. Yamaguchi, eds. Biomathematics Series, Vol. 71. Springer-Verlag, Berlin, pp. 32–47.

Olson, D. B., G. L. Hitchcock, A. J. Mariano, C. J. Ashjian, G. Peng, R. W. Nero and G. P. Podesta, 1994. Life on the edge: marine life and fronts. *Oceanography*, **7,** 52–60.

Osborn, T. R., 1998. Finestructure, microstructure, and thin layers. *Oceanography*, **11,** 36–43.

Osborn, T. R., D. M. Farmer, S. Vagle, S. A. Thorpe and M. Cure, 1992. Measurements of bubble plumes and turbulence from a submarine. *Atmos. Oceans*, **30,** 419–440.

Owen, R. W., 1989. Microscale and finescale variations of small plankton in coastal and pelagic environments. *J. Mar. Res.*, **47,** 197–240.

Paffenhofer, G. A., J. R. Strickler and M. Alcaraz, 1982. Suspension feeding by herbivorous copepods: a cinematographic study. *Mar. Biol.*, **67,** 193–199.

Peters, H., M. C. Gregg and J. M. Toole, 1988. On the parameterization of equatorial turbulence. *J. Geophys. Res.*, **93,** 1199–1218.

Pinel-Alloul, B., 1995. Spatial heterogeneity as a multiscale characteristic of zooplankton community. *Hydrobiology*, **300–301,** 17–42.

Pinkel, R. and J. A. Smith, 1987. Open ocean surface wave measurement using Doppler sonar. *J. Geophys. Res.*, **92,** 12967–12973.

Pollard, R. T., 1977. Observations and theories of Langmuir circulations and their role in near surface mixing. In *A Voyage of Discovery: George Deacon 70th Anniversary Volume*, M. Angel, ed. Pergamon Press, Elmsford, N.Y., pp. 235–251.

Poulet, S. and G. Ouellet, 1982. The role of amino acids in the chemosensory swarming and feeding behavior of marine copepods. *J. Plankton Res.*, **4,** 341–361.

Price, J. F., 1981. Upper ocean response to a hurricane. *J. Phys. Oceanogr.*, **11,** 153–175.

Price, J. F., 1983. Internal wave wake of a moving storm. I. Scales, energy budget and observations. *J. Phys. Oceanogr.*, **13,** 949–965.

Price, J. F., R. A. Weller and R. Pinkel, 1986. Diurnal cycling: observations and models of the upper ocean response to diurnal heating, cooling, and wind mixing. *J. Geophys. Res.*, **91,** 8411–8427.

Prunet, P., J.-F. Minster, D. Ruiz-Piño and I. Dadou, 1996. Assimilation of surface data in a one-dimensional physical–biogeochemical model of the surface ocean. 1. Method and preliminary results. *Global Biogeochem. Cycles*, **10,** 111–138.

Riley, G. A., 1946. Factors controlling phytoplankton populations on Georges Bank. *J. Mar. Res.*, **6,** 54–73.

Riley, G. A., 1947. A theoretical analysis of the zooplankton population of Georges Bank. *J. Mar. Res.*, **6,** 104–113.

Rothschild, B. J. and T. R. Osborn, 1988. Small-scale turbulence and planktonic contact rates. *J. Plankton Res.*, **10,** 465–474.

Saiz, E. and M. Alcaraz, 1992. Free-swimming behaviour of *Acartia clausi* (Copepoda: Calanoida) under turbulent water movement. *Mar. Ecol. Prog. Ser.* **80,** 229–236.

Saiz, E., P. Tiselius, P. R. Johnson, P. Verity and G.-A. Paffenhöfer, 1993. Experimental records of the effects of food patchiness and predation of egg production of *Acartia tonsa. Limnol. Oceanogr.*, **38,** 280–289.

Sarmiento, J. L., R. D. Slater, M. J. R. Fasham, H. W. Ducklow, J. R. Toggweiler and G. T. Evans, 1993. A seasonal three-dimensional ecosystem model of nitrogen cycling in the North Atlantic euphotic zone. *Global Biogeochem. Cycles*, **7,** 379–415.

Shay, T. J. and M. C. Gregg, 1986. Convectively driven turbulent mixing in the upper ocean. *J. Phys. Oceanogr.*, **16,** 1777–1798.

Sieracki, M. E., D. J. Gifford, S. M. Gallagher and C. S. Davis, 1998. Ecology of a *Chaetoceros socialis* (Lauder) patch on Georges Bank: distribution, microbial associations, and grazing losses. *Oceanography*, **11,** 30–35.

Siggia, E. D., 1981. Numerical study of small scale intermittency in three dimensional turbulence. *J. Fluid Mech.*, **107,** 375–406.

Skyllingstad, E. D. and D. W. Denbo, 1995. An ocean large-eddy simulation of Langmuir circulations and convection in the surface mixed layer. *J. Geophys. Res.*, **100,** 8501–8522.

Smith, J., 1992. Observed growth of Langmuir circulation. *J. Geophys. Res.*, **97,** 5651–5664.

Squires, K. and J. K. Eaton, 1991. Preferential concentration of particles by turbulence. *Phys. Fluids A*, **3,** 1169–1176.

Squires, K. and H. Yamazaki, 1995. Preferential concentration of marine particles in isotropic turbulence. *Deep Sea Res.*, **42,** 1989–2004.

Steele, J. H., 1974. *The Structure of Marine Ecosystems.* Harvard University Press, Cambridge, Mass.

Stewart, R. W., 1969. *Turbulence* (motion picture file). Educational Services, Inc., Cambridge, Mass.

Strickler, J. R., 1977. Observation of swimming performances of planktonic copepods. *Liminol. Oceanogr.*, **22,** 165–170.

Strickler, J. R., 1982. Calanoid copepods, feeding currents, and the role of gravity. *Science*, **218,** 158–160.

Strickler, J. R., 1985. Feeding currents in calanoid copepods: two new hypotheses. In *Physiological Adaptations of Marine Animals*, M. S. Laverack, ed. *Symp. Soc. Exp. Biol.*, **39,** 459–485.

Strickler, J. R., 1998. Observing free-swimming copepods mating. *Philos. Trans. R. Soc. London Ser. B*, **353,** 671–680.

Sundby, S., 1997. Turbulence and icthyoplankton: influence on vertical distributions and encounter rates. *Sci. Mar.*, **61**(Suppl. 1), 159–176.

Tandon, A. and S. Leibovich, 1995. Secondary instabilities in Langmuir circulations. *J. Phys. Oceanogr.*, **25,** 1206–1217.

Taylor, G. I., 1921. Diffusion by continuous movements. *Proc. London Math. Soc.*, **20,** 196–211.

Tennekes, H. and J. L. Lumley, 1990. *A First Course in Turbulence*. MIT Press, Cambridge, Mass.

Thorpe, S. A., 1977. Turbulence and mixing in a Scottish loch. *Philos. Trans. R. Soc. London Ser. A*, **286,** 125–181.

Thorpe, S. A., 1984. The effect of Langmuir circulation on the distribution of submerged bubbles caused by breaking waves. *J. Fluid Mech.*, **142,** 151–170.

Thorpe, S. A., 1985. Small-scale processes in the upper ocean boundary layer. *Nature*, **318,** 519–522.

Tiselius, P., 1992. Behavior of *Acacia tonsa* in patch food environments. *Limnol. Oceanogr.*, **37,** 1640–1651.

Tiselius, P., 1998. An *in situ* video camera for plankton studies, design and preliminary observations. *Mar. Ecol. Prog. Ser.*, **164,** 293–299.

Tiselius, P. and P. R. Jonsson, 1990. Foraging behavior of six calanoid copepods: observations and hydrodynamic analysis. *Mar. Ecol. Prog. Ser.*, **66,** 23–33.

van Duren, L. E., E. J. Stamhuis and J. J. Videler, 1998. Reading the copepod personal ads: increasing encounter probability with hydromechanical signals. *Phil. Trans. R. Soc. London Ser. B*, **353,** 691–700.

Viitasalo, M., T. Kiorboe, J. Flinkman, L. W. Pederson, and A. W. Visser, 1998. Predation vulnerability of planktonic copepods: consequences of predator foraging strategies and prey sensory abilities. *Mar. Ecol. Prog. Ser.*, **175,** 129–142.

Vincent, A. and M. Meneguzzi, 1991. The spatial structure and statistical properties of homogeneous turbulence. *J. Fluid Mech.*, **225,** 1–20.

Visser, A. W., 1997. Using random walk models to simulate the vertical distribution of particles in a turbulent water column. *Mar. Ecol. Prog. Ser.*, **158,** 275–281.

Walsh, J. J., 1975. A spatial simulation model of the Peru upwelling ecosystem. *Deep-Sea Res.*, **22,** 201–236.

Weissburg, M. J., M. H. Doall and J. Yen, 1998. Following the invisible trail: kinematic analysis of mate-tracking in the copepod *Temora longicornis. Philos. Trans. R. Soc. London Ser. B*, **353,** 671–680.

Weller, R. A. and J. F. Price, 1988. Langmuir circulation within the oceanic mixed layer. *Deep-Sea Res.*, **35,** 711–747.

Weller, R. A., J. P. Dean, J. Marra, J. Prices, E. A. Francis and D. C. Boardman, 1985. Three-dimensional flow in the upper ocean. *Science*, **227,** 1552–1556.

Werner, F. E. and J. F. Gilliam, 1984. The ontogenetic niche and species interactions in size-structures populations. *Annu. Rev. Ecol. Syst.*, **15,** 393–425.

Werner, F. E., F. H. Page, D. R. Lynch, J. W. Loder, R. G. Lough, R. I. Perry, D. A. Greenberg and M. M. Sinclair, 1993. Influences of mean advection and simple behavior on the distribution of cod and haddock early life stages on Georges Bank. *Fish. Oceanogr.*, **2,** 43–64.

Wiggert, J. D., B. H. Jones, J. T. Dickey, K. H. Brink, R. A. Weller, J. Marra and L. A. Codispoti, 2000. The Northeast Monsoon's impact on mixing, phytoplankton biomass and nutrient cycling in the Arabian Sea. *Deep-Sea Res. II*, **47,** 1353–1385.

Woods, J. D. and W. Barkmann, 1986. The response of the upper ocean to solar heating. I. The mixed layer. *Q. J. R. Meteorol. Soc.*, **112,** 1–27.

Woods, J. D. and R. Onken, 1982. Diurnal variation and primary production in the ocean: preliminary results of a Lagrangian ensemble model. *J. Plankton Res.*, **4,** 735–756.

Wroblewski, J. S., 1980. A simulation of the distribution of *Acartia clausi* during Oregon upwelling, August 1973. *J. Plankton Res.*, **2,** 43–68.

Wroblewski, J. S. and J. J. O'Brien, 1976. A spatial model of phytoplankton patchiness. *Mar. Biol.*, **35,** 161–175.

Yamazaki, H., 1990. Breakage models: lognormality and intermittency. *J. Fluid Mech.*, **219,** 181–193.

Yamazaki, H., 1993. Lagrangian study of planktonic organisms: perspectives. *Bull. Mar. Sci.*, **53,** 265–278.

Yamazaki, H. and L. R. Haury, 1993. A new Lagrangian model to study animal aggregation. *Ecol. Model.*, **69,** 99–111.

Yamazaki, H. and D. Kamykowski, 1991. The vertical trajectories of motile phytoplankton in a wind-mixed water column. *Deep-Sea Res.*, **38,** 219–241.

Yamazaki, H. and D. Kamykowski, 1994. Reply to Greg Holloway. *Deep-Sea Res. I*, **41,** 961–963.

Yamazaki, A. K. and D. Kamykowski, 2000. A dinoflagellate adaptive behavior model: response to internal biochemical cues. *Ecol. Model.*, **134,** 59–72.

Yamazaki, H. and R. Lueck, 1987. Turbulence in the California undercurrent, *J. Phys. Oceanogr.*, **17,** 1378–1396.

Yamazaki, H. and R. Lueck, 1990. Why oceanic dissipation rates are not lognormal. *J. Phys. Oceanogr.*, **20,** 1907–1918.

Yamazaki, H. and A. Okubo, 1995. A simulation of grouping: an aggregating random walk. *Ecol. Model.*, **79,** 159–165.

Yamazaki, H. and T. R. Osborn, 1988. Review of oceanic turbulence: implication for biodynamics. In *Toward a Theory on Biological–Physical Interactions in the World Ocean*, B. J. Rothschild, ed. D. Reidel, Dordrecht, The Netherlands, pp. 215–233.

Yamazaki, H. and K. D. Squires, 1996. Comparison of oceanic turbulence and copepod swimming. *Mar. Ecol. Prog. Ser.*, **144,** 299–301.

Yamazaki, H., T. R. Osborn and K. D. Squires, 1991. Direct numerical simulation of planktonic contact in turbulent flow. *J. Plankton Res.*, **13,** 629–643.

Yen, J., 1988. Directionality and swimming speeds in predatory–prey and male–female interactions of *Euchaeta rimana*, a subtropical marine copepod. *Bull. Mar. Sci.*, **43,** 395–403.

Yen, J. and D. M. Fields, 1992. Escape responses of *Acartia hudsonica* (Copepoda) nauplii from the flow field of *Temora longicornis* (Copepoda). *Arch. Hydrobiol. Beih.*, **36,** 123–134.

Yen, J. and N. T. Nicoll, 1990. Setal array on the first antennae of a carnivorous marine copepod, *Euchaeta norvegica. J. Crustac. Biol.*, **10,** 218–224.

Yen, J. and J. R. Strickler, 1996. Advertisement and concealment in the plankton: what makes a copepod hydrodynamically conspicuous? *Invertebr. Biol.*, **115,** 191–205.

Yen, J., P. H. Lenz, D. V. Grassie and D. K. Hartline, 1992. Mechanoreception in marine copepods: electrophysiological studies on the first antennae. *J. Plankton Res.*, **14,** 495–512.

Yen, J., M. J. Weissburg and M. H. Doall, 1998. The fluid physics of signal perception by mate-tracking copepods. *Philos. Trans. R. Soc. London Ser. B*, **353,** 787–804.

Zahariev, K., 1998. Dynamics and modelling of the oceanic surface boundary layer. Ph.D. dissertation. University of Victoria, Victoria, British Columbia, Canada.

Zedel, L. and D. M. Farmer, 1991. Organized structures in subsurface bubble clouds: Langmuir circulation in the open ocean. *J. Geophys. Res.*, **96,** 8889–8900.